Cosmological test of $\frac{\sigma}{\theta}$ as function of scale factor in $f(R,T)$ framework

A DISSERTATION

SUBMITTED IN PARTIAL FULFILLMENT OF THE REQUIREMENTS
FOR THE AWARD OF THE DEGREE
OF

MASTER OF SCIENCE
IN
[**MATHEMATICS**]

Submitted by :

[**Himanshu Chaudhary**]**(2K21/MSCMAT/21)**
[**Ankita Kohli**]**(2K21/MSCMAT/02)**

Under the supervision of

[Prof.Aditya Kaushik]

DEPARTMENT OF APPLIED MATHEMATICS
DELHI TECHNOLOGICAL UNIVERSITY

(Formerly Delhi College of Engineering)
Bawana Road,Delhi -110042

7 MAY 2022

CANDIDATE'S DECLARATION

We (Himanshu Chaudhary),2K21/MSCMAT/21 and (Ankita Kohli), 2K21/MSCMAT/02 of M.Sc(Applied Mathematics), hereby declare that the project Dissertation titled "Cosmological test of $\frac{\sigma}{\theta}$ as a function of scale factor in $f(R,T)$ framework" which is submitted by us to the Department of Applied Mathematics, Delhi Technological University, Delhi in partial fulfillment of the requirement for the award of the degree of Master of Science is original and not copied from any source without proper citation. This work has not previously formed the basis for awarding any Degree, Diploma Associateship, Fellowship, or other similar title or recognition.

Place: Delhi
Date:

Himanshu Chaudhary

Ankita Kohli

Supervisor
Prof. Aditya Kaushik
Department of Applied Mathematics
Delhi Technological University

CERTIFICATE

We hereby certify that the project Dissertation titled "Cosmological test of $\frac{\sigma}{\theta}$ as a function of scale factor in $f(R,T)$ framework " which is submitted by Himanshu Chaudhary (2K21/MSCMAT/21) and Ankita Kohli(2K21/MSCMAT/02) to the department of Applied Mathematics, this document submitted to Delhi Technological University as part of the requirements for the Master of Science degree,is the record of project work, completed by students under my supervision. This thesis has not been applied in part or full for any degree or diploma at the university or elsewhere, to the best of my knowledge.

Place: Delhi
Date:

Prof. Aditya Kaushik
Department of Applied Mathematics
Delhi Technological University

ACKNOWLEDGEMENT

I would like to take this opportunity to express my heartfelt gratitude to all those who have contributed to the successful completion of this research report. Their support, guidance, and encouragement have been invaluable throughout this journey. I extend my deepest appreciation to Professor Mr. Aditya Kaushik for his exceptional mentorship and invaluable guidance. His profound knowledge, insightful feedback, and unwavering support have played a pivotal role in shaping the research topics and methodology of this report. His encouragement and constructive criticism have consistently pushed me to elevate the quality of my work, and I am immensely grateful for his mentorship. I would also like to express my sincere thanks to God and my parents for their unwavering support, love, and understanding. Their wise counsel, encouragement, and belief in my abilities have been a constant source of inspiration throughout this journey. I am forever grateful for their sacrifices and the opportunities they have provided me. I am indebted to my friends and colleagues who have been a source of motivation and support. Their valuable discussions, suggestions, and encouragement have significantly enriched my understanding and have been instrumental in shaping the ideas presented in this report. I would like to acknowledge the contributions of all the researchers and scholars whose work and publications have formed the foundation of this research. Their dedication to advancing knowledge in the field of [mention the field] has provided the necessary framework for my own exploration and analysis. I would like to express my appreciation to all the individuals who directly or indirectly supported me during the research and writing process. Their contributions, whether big or small, have been invaluable and have helped shape the final outcome of this research report. I am deeply grateful to everyone who has been a part of this research journey. Your support, guidance, and encouragement have been pivotal in bringing this report to fruition. Thank you for believing in me and for being an integral part of my academic and personal growth.

ABSTRACT

This study investigates the Bianchi type-I space-time model with perfect fluid in the context of the modified theory of gravity, specifically the $f(R,T)$ modified theory. Here, R represents the Ricci scalar, and T denotes the trace of the energy-momentum tensor. The gravitational field equations corresponding to the $f(R,T)$ theory are solved by considering expansion anisotropy as a function of the average scale factor. The analysis involves estimating the best-fit values of the model parameters through the use of a combined dataset comprising Cosmic Chronometers (CC) measurements (31 data points), a type Ia supernova dataset (1048 data points), and a Baryon Acoustic Oscillations dataset (ten measurements). The Markov Chain Monte Carlo (MCMC) method is employed for parameter estimation. The obtained results reveal that the deceleration parameter of the Universe underwent an initial decelerated phase followed by a transition to an accelerated phase. Additionally, the study explores cosmographic and cosmological parameters, proposes potential improvements, and presents the findings using diagrams. Overall, this investigation contributes to our understanding of the Bianchi type-I space-time model in the framework of the $f(R,T)$ modified theory of gravity and provides valuable insights into the evolution and dynamics of the Universe.

Contents

1 Chapter 1

1.1 Introduction

In 1917, Albert Einstein introduced the Cosmological Constant Λ into his field equations of general relativity [1]. He introduced this term to achieve a static Universe, as the prevailing view at the time was that the Universe was unchanging and finite in size. By adding the Cosmological Constant, Einstein hoped to counteract the gravitational attraction between matter and ensure a static, balanced Universe. However, in 1922, Alexander Friedmann derived the two Friedmann equations that described the evolution of the Universe's spatial scale over time [2]. These equations showed that the Universe could indeed expand or contract, contrary to Einstein's static Universe hypothesis. In 1927 and 1929, Georges Lemaitre and Edwin Hubble, respectively, independently observed the redshift of light from distant galaxies, realizing that it was a consequence of the expansion of the Universe [3, 4]. This discovery indicated that the Universe was not static but was actually expanding, leading to the formulation of the Big Bang theory, which posits that the Universe began from an extremely hot and dense state. Further evidence supporting the expanding Universe and the Big Bang theory came in 1964 with the discovery of Cosmic Microwave Background Radiation (CMB) by Arno Allan Penzias and Robert Woodrow Wilson [5]. The CMB is a faint, uniform radiation that permeates the entire Universe and is a remnant of the early hot and dense phase. Its detection provided strong support for the Big Bang theory. In 1998, observations of distant supernovae by the Supernova Cosmology Project and the High-Z Supernova Search Team revealed that the expansion of the Universe is accelerating, contrary to expectations [6, 7]. This discovery led to the realization that there must be an additional energy component driving this accelerated expansion, which is now referred to as dark energy. The term "dark energy" is often used to describe the energy associated with the Cosmological Constant Λ. In the Einstein Field Equations, when Λ is on the left side along with the curvature term, it influences the overall geometry of space-time and acts as a repulsive force, contributing to the accelerated expansion [8]. To further confirm the accelerating expansion of the Universe, various astrophysical observations have been conducted. One such example is the Baryon Oscillation Spectroscopic Survey (BOSS) conducted by the WiggleZ collaboration [9]. Additionally, the Planck satellite mission, a collaboration between the European Space Agency (ESA) and other international partners, has made precise measurements of the CMB, providing valuable data on the properties of dark energy and the overall composition of the Universe [10]. The inclusion of the Cosmological Constant Λ in Einstein's field equations, initially proposed for a static Universe, eventually led to the realization that the Universe is expanding. Observations of redshifted light from distant galaxies, the discovery of the CMB, and subsequent studies of supernovae all pointed to an expanding Universe. The accelerated expansion observed in 1998 indicated the existence of dark energy, associated with the small but positive value of Λ. This dark energy, often referred to as the Cosmological Constant, drives accelerated expansion and has properties that distinguish it from ordinary matter. Ongoing research, utilizing techniques such as BAO and measurements from the Planck satellite, continues to deepen our understanding of dark energy and its role in shaping the Universe.

1.2   About $f(R,T)$ modified gravity

In the realm of fundamental physical theories, action principles play a crucial role by providing intrinsic descriptions that are independent of coordinate choices. In the context of gravity, the metric action is particularly significant as it is defined intrinsically. Space-time is considered a manifold denoted by M with a Lorentzian signature metric, and the action is evaluated by integrating across this manifold. The simplest scalar function that can be used in the action is the Ricci scalar R, which is associated with the Einstein-Hilbert action. However, the $f(R,T)$ modified theory of gravity, proposed by Harko et al. [11], introduces a modification to the conventional Einstein-Hilbert action [12, 13, 14, 15, 16, 17, 18, 19, 20, 21, 22]. In this modified theory, R represents the curvature scalar, and T corresponds to the trace of the Stress-Energy Momentum tensor. The motivation behind this theory is to provide an explanation for the observed late-time acceleration of the Universe without the need to introduce the cosmological constant Λ. Since its proposal, the $f(R,T)$ modified theory of gravity has gained significant attention among theoretical cosmologists for its ability to address various cosmological issues. It offers an alternative framework to explain phenomena that were traditionally attributed to dark energy and modified gravity theories. To further elaborate on the $f(R,T)$ modified theory of gravity, it is essential to explore its specific details and implications. This theory encompasses a broader range of cosmological phenomena, and its formulations have been applied to address questions related to the early Universe, dark matter, and the accelerated expansion of the Universe.

1.3   Bianchi Universe

Bianchi universes, named after Luigi Bianchi who classified the relevant three-dimensional spaces, are a class of cosmological models that exhibit homogeneity but not necessarily isotropy on spatial slices. Within this class, we find the well-known Friedmann-Lemaître-Robertson-Walker (FLRW) universes as a special subclass, which are isotropic and homogeneous. One of the significant aspects of studying Bianchi models is their comparison with observational data from the real Universe. Calculations involving nucleosynthesis and microwave background anisotropies in Bianchi models have been performed, aiming to detect any potential anisotropy. However, these analyses have generally yielded null results, leading to upper limits on the level of anisotropy present. Notably, the findings of Jaffe et al. in 2005 [23] tentatively suggested non-zero anisotropic shear in certain Bianchi models. However, subsequent studies, such as those by the Planck Collaboration in 2015 [24], and investigations into the polarization of the microwave background conducted by Pontzen and Challinor in 2007 [25], have cast doubts on the consistency of these detections with other well-established cosmological parameters. Despite the challenges associated with observational constraints, Bianchi's models continue to be widely studied for their pedagogical value. One of their key advantages is that the spatial homogeneity of these models simplifies the Einstein equations, reducing them from partial to ordinary differential equations in time. This feature makes Bianchi's models tractable and provides exact solutions to Einstein's field equations. In addition to the general class of Bianchi models, Bianchi-type spacetime-1 (Bianchi-I) deserves special mention. Bianchi-I represents a specific subclass of Bianchi models characterized by anisotropic expansion in three

orthogonal spatial directions. The Bianchi-I spacetime exhibits different expansion rates along these directions, resulting in anisotropic behavior.

1.4 Motivation

The discovery of anisotropies in the cosmic microwave background (CMB) radiation has led to the exploration of anisotropic universe models, including those within the Bianchi-type framework. In light of this, my research work aims to investigate the implications of the $f(R,T)$ modified theory of gravity in the context of anisotropic cosmological models. By solving the gravitational field equations derived from the $f(R,T)$ theory, I examine the behavior of the resulting deceleration parameter. The deceleration parameter provides crucial insights into the expansion dynamics of the Universe. The analysis reveals that in the framework of $f(R,T)$ gravity, the Universe experiences an initial decelerated expansion phase followed by a transition to an accelerated expansion phase. This observation highlights the ability of the modified theory to account for the observed transition from deceleration to acceleration in the evolution of the Universe. Additionally, I delve into the study of cosmographic and cosmological parameters within the $f(R,T)$ modified gravity framework. These parameters serve as essential tools for characterizing the cosmological dynamics and evolution of the Universe. Through my research, I aim to refine and enhance existing cosmographic and cosmological parameterizations, providing a deeper understanding of the behavior and implications of the $f(R,T)$ modified theory of gravity in the context of anisotropic cosmological models. To effectively present the outcomes of my research, I employ illustrative diagrams and figures that visually convey the obtained results. These visual representations aid in comprehending the behavior of the cosmographic and cosmological parameters, thereby facilitating a more intuitive interpretation of the findings.

1.5 Related Work

In the context of $f(R,T)$ gravity, several studies have explored the properties of Bianchi type-I and anisotropic Bianchi type-VI_0 spacetimes, considering different matter sources and investigating the physical behavior of these models. Adhav [28] derived exact solutions of the field equations for a locally rotationally symmetric (LRS) Bianchi type-I spacetime filled with a perfect fluid within the framework of $f(R,T)$ gravity. The author examined the physical behavior of the model and discussed the impact of the $f(R,T)$ function on the matter distribution. Neelima and Rao [29] studied the spatially homogeneous and anisotropic Bianchi type-VI_0 spacetime filled with a perfect fluid. They analyzed the model within the framework of $f(R,T)$ gravity proposed by Harko et al. [11]. The field equations were solved, taking advantage of the anisotropy feature of the universe in Bianchi type-VI_0 spacetime. The authors observed that the inclusion of the $f(R,T)$ function did not significantly impact the geometry of spacetime but had slight effects on the matter distribution. Shamir [30] investigated the locally rotationally symmetric (LRS) Bianchi type-I universe in the framework of $f(R,T)$ gravity. The author obtained exact solutions of the modified field equations by assuming an expansion scalar proportional to the shear scalar. The study focused on

the exact solutions of the locally rotationally symmetric Bianchi type-I spacetime. Sahoo and Sivakumar [31] explored locally rotationally symmetric (LRS) Bianchi type-I cosmological models. They derived exact solutions of the field equations considering a linearly varying deceleration parameter. The authors investigated the dynamic and physical behavior of the models, highlighting that one of the models exhibited a "big rip" scenario, suggesting that the linearly varying deceleration parameter might inherently lead to such a cosmic fate.vTiwari et al. [32] considered the Bianchi type-I model in the framework of $f(R, T)$ gravity, incorporating fluctuating gravitational and cosmological constants. They took $f(R, T) = R + 2f(T)$ and assumed a linear relation between the deceleration parameter and the Hubble parameter. The study examined the cosmological implications of the model. Tiwari and Beesham [33] investigated a spatially homogeneous and anisotropic locally rotationally symmetric Bianchi type-I spacetime with a cosmological term in $f(R, T)$ gravity. They obtained solutions of the field equations under a variation law for the Hubble parameter, studying the anisotropic properties of the model. Singh and Beesham [34] incorporated a primary matter source and examined the LRS Bianchi type-I model in the framework of $f(R, T)$ gravity. The coupling between matter and $f(R, T)$ gravity introduced an additional matter source. The authors obtained constraints for a realistic cosmological scenario and considered the case of a scalar field (normal or phantom) model, concluding that the model is consistent with a phantom scalar field only. These studies contribute to the understanding of the behavior and properties of Bianchi type-I and anisotropic Bianchi type-VI_0 spacetimes within the framework of $f(R, T)$ gravity, providing insights into the impact of the $f(R, T)$ function and the matter distribution on the evolution of the universe.

1.6 Overview

This paper presents a comprehensive investigation of the Bianchi type-I cosmological model within the framework of the $f(R, T)$ theory of gravity. Our analysis aims to explore the effects of anisotropy in the context of a perfect fluid-filling spacetime. Anisotropy is considered to be proportional to a function expressed in terms of the scale factor, which is motivated by the presence of minor temperature fluctuations in the cosmic microwave background (CMB), a remnant of the early universe. These temperature fluctuations indicate the existence of anisotropy, which has both theoretical support and is confirmed by contemporary experimental results. The study of anisotropic cosmological models is crucial for understanding the early universe and its subsequent evolution. By investigating the Bianchi type-I model, we aim to gain insights into the behavior of an anisotropic universe and its implications for the $f(R, T)$ theory of gravity. This theory offers an extended framework beyond the standard general relativity by incorporating a coupling between the curvature scalar R and the trace of the stress-energy momentum tensor T. Our research is motivated by the need to understand the interplay between anisotropy and the $f(R, T)$ theory in cosmology. By considering a perfect fluid as the matter content of the universe, we can explore the dynamics and evolution of an anisotropic universe in the context of this modified gravity theory. This analysis will provide valuable insights into the behavior of cosmic structures and the overall evolution of the universe. To support our investigation, we draw

upon the theoretical foundations of the $f(R, T)$ theory of gravity, which has been extensively studied in the literature [26, 27]. Additionally, contemporary experimental results further support the existence of anisotropy in the universe, providing a strong motivation for exploring its implications within the $f(R, T)$ framework.

2 Chapter 2

2.1 Review of $f(R,T)$ and field equations in Bianchi type-I space-time

The gravitational action for the modified $f(R,T)$ theory of gravity takes the form [11]

$$S = \int \left(\frac{1}{16\pi} f(R,T) + S_m \right) \sqrt{-g} dx^4, \tag{1}$$

where $f(R,T)$ is an arbitrary function of the Ricci scalar R and the trace T of the energy momentum tensor T_{ij}. Harko et al. [?] proposed three classes as

$$f(R,T) = \begin{cases} R + 2h(T), \\ h_1(R) + h_2(T) \\ h_1(R) + h_2(R)h_3(T). \end{cases} \tag{2}$$

However, we restrict ourselves to $f(R,T) = R + 2h(T)$ and put $h(T) = \alpha T$, where α is the coupling constant. Then,
equation (??) leads to

$$f_R(R,T)R_{ij} - \frac{1}{2}f(R,T)g_{ij} + (g_{ij} - \nabla_i\nabla_j)f_R(R,T) = 8\pi T_{ij} - f_T(R,T)T_{ij} - f_T(R,T)\Theta_{ij}. \tag{3}$$

Here, $= \nabla^i\nabla_j$ is the D'Alembert operator and $\Theta_{ij} = g^{ml}\dfrac{\delta T_{ml}}{\delta g^{ij}}$. Suppose that the matter in the Universe is a perfect fluid hence

$$\Theta_{ij} = -2T_{ij} - pg_{ij}$$

where $T_{ij} := (\rho + p)u_iu_j - pg_{ij}$ is the energy-momentum tensor with perfect fluid, ρ and p are energy density and cosmic pressure. Moreover, u^i is the four-velocity vector such that $u^iu_i = 1$. Consequently, the field equation takes the form

$$R_{ij} - \frac{1}{2}Rg_{ij} = 8\pi T_{ij} + 2f_T T_{ij} + [f(T) + 2pf_T]g_{ij}. \tag{4}$$

The Bianchi type-I model of the Universe reads

$$ds^2 = -dt^2 + A^2dx^2 + B^2dy^2 + C^2dz^2, \tag{5}$$

where A, B and C are the scale factors and function of time t only. The modified field equations are obtained as

$$\dot{H}_2 + H_2^2 + \dot{H}_3 + H_3^2 + H_2H_3 = -(8\pi + 3\alpha)p + \alpha\rho, \tag{6}$$

$$\dot{H}_1 + H_1^2 + \dot{H}_3 + H_3^2 + H_1H_3 = -(8\pi + 3\alpha)p + \alpha\rho, \tag{7}$$

$$\dot{H}_1 + H_1^2 + \dot{H}_2 + H_2^2 + H_1H_2 = -(8\pi + 3\alpha)p + \alpha\rho, \tag{8}$$

$$H_1H_2 + H_2H_3 + H_3H_1 = (8\pi + 3\alpha)\rho - \alpha p, \tag{9}$$

where $H_1 = \dfrac{\dot{A}}{A}$, $H_2 = \dfrac{\dot{B}}{B}$ and $H_3 = \dfrac{\dot{C}}{C}$.

The average scale factor a and the volume V for the Bianchi type-I model are given by

$$V = a^3 = ABC. \tag{10}$$

Using (9) and (10) to write

$$(\dot{H}_1 + H_1^2) - (\dot{H}_2 + H_2^2) - H_3(H_1 - H_2) = 0. \tag{11}$$

Integration leads to

$$H_1 - H_2 = \frac{k_1}{a^3} \tag{12}$$

for some constant k_1. Again, using (10) and (11) to obtain

$$H_2 - H_3 = \frac{k_2}{a^3} \tag{13}$$

where k_2 is another constant of integration. From (11), (12) and (13), it follows that

$$H_1 = \frac{\dot{a}}{a} + \frac{(2k_1 + k_2)}{3a^3}, \quad H_2 = \frac{\dot{a}}{a} + \frac{(k_2 - k_1)}{3a^3}, \quad \text{and} \quad H_3 = \frac{\dot{a}}{a} - \frac{(k_1 + 2k_2)}{3a^3}. \tag{14}$$

The Hubble parameter H, deceleration parameter q and shear tensor σ_{ij} for Bianchi type-I model are defined as

$$H = \frac{\dot{a}}{a}, \quad q = \frac{d}{dt}\left(\frac{1}{H}\right) - 1, \quad \text{and} \quad \sigma_{ij} = \frac{1}{2}\sigma_{ij}\sigma^{ij}, \tag{15}$$

$$\sigma_{11} = H_1 - H = \frac{(2k_1 + k_2)}{3a^3}, \tag{16}$$

$$\sigma_{22} = H_2 - H = \frac{(k_2 - k_1)}{3a^3}, \tag{17}$$

$$\sigma_{33} = H_3 - H = \frac{(k_1 + 2k_2)}{3a^3}, \tag{18}$$

$$\sigma_{44} = 0. \tag{19}$$

$$\sigma = \frac{1}{2}(\sigma_{11}^2 + \sigma_{22}^2 + \sigma_{33}^2 + \sigma_{44}^2) = \frac{k}{a^3}, \tag{20}$$

where $3k^2 = k_1^2 + k_2^2 + k_1 k_2$. Substitute values from (14) into (6)-(9) to obtain the pressure p and energy density ρ as

$$p = \frac{-1}{[(8\pi + 3\alpha)^2 - \alpha^2]}\left[2(8\pi + 3\alpha)\frac{\ddot{a}}{a} + 8\pi\left(\frac{\dot{a}}{a}\right)^2 + \frac{(8\pi + 4\alpha)k^2}{a^6}\right] \tag{21}$$

and

$$\rho = \frac{1}{[(8\pi + 3\alpha)^2 - \alpha^2]}\left[-2\alpha\frac{\ddot{a}}{a} + (24\pi + 8\alpha)\left(\frac{\dot{a}}{a}\right)^2 - \frac{(8\pi + 4\alpha)k^2}{a^6}\right]. \tag{22}$$

2.2 Solutions of the field equations

Let us consider the anisotropy $\left(\frac{\sigma}{\theta}\right)$ as a function of scale factor $a(t)$ and $\theta = 3H$. Suppose it is astronomically immense at the beginning of the Universe and vanishes for extensively large t. For Bianchi type-I spacetime, we have

$$\frac{\sigma}{\theta} = \frac{k}{3a^2\dot{a}} = f(a). \tag{23}$$

Integrating, we get

$$k(t + t_1) = 3\int a^2 f(a) da \tag{24}$$

where t_1 is a constant of integration. Following [?], let

$$f(a) = \frac{1}{(n + a^3)} \tag{25}$$

where n is a positive integer. For this choice of function, observe that at an earlier time $\frac{\sigma}{\theta} \neq 0$ and at a later time $\frac{\sigma}{\theta} = 0$. Consequently, from ((28)) and ((29)) the scale factor of the Universe is obtained as

$$a = [n(e^{kt} - 1)]^{\frac{1}{3}}. \tag{26}$$

Keep in mind that $k = 0$ is a singular point. In the current paper and $k > 0$. Next, we use the relation $H = \frac{\dot{a}}{a}$ and equation (26) to write

$$H = \frac{\dot{a}}{a} = \frac{k}{3}\left[\frac{e^{kt}}{e^{kt} - 1}\right]. \tag{27}$$

Using (26) and relation $a = \frac{1}{1+z}$ to obtain redshift-time relation

$$t = \frac{1}{k}log\left[\frac{n(1+z)^3 + 1}{n(1+z)^3}\right]. \tag{28}$$

Consequently, the Hubble parameter in terms of the redshift, reads

$$H(z) = \frac{k}{3}(n(z+1)^3 + 1). \tag{29}$$

The deceleration parameter q is given by

$$q = \frac{d}{dt}\left(\frac{1}{H}\right) - 1. \tag{30}$$

Therefore, from (27) and (30), we obtain

$$q = -1 + 3e^{-kt}. \tag{31}$$

Moreover, the deceleration parameter in terms of the redshift is obtained using (27) in (31) as

$$q = \frac{-1 + 2n(z+1)^3}{1 + n(z+1)^3}. \tag{32}$$

3 Chapter 3

3.1 Cosmological tests of the $\frac{\sigma}{\theta}$ as function of scale factor

In this section, we aim to perform a comprehensive analysis of our cosmological model by comparing its predictions to observational data and constraining the model parameters. We utilize three distinct observational datasets: the Cosmic Chronometers data, the Supernova datasets consisting of 1048 points, and the Baryon Acoustic Oscillations (BAO). By comparing our model's predictions with these cosmological data sets, we aim to determine the best-fit parameter ranges for our model. To constrain the parameters of our cosmological model, we employ the standard Bayesian technique, along with a likelihood function approach, using the Markov Chain Monte Carlo (MCMC) method. These methods allow us to statistically analyze the data and obtain the most probable values for the model parameters that are consistent with the observations. Once we have determined the best-fit values for the model parameters, we proceed to investigate the cosmological model from a cosmographic perspective. This analysis involves studying the evolution of various cosmographic parameters, such as the deceleration parameter, jerk parameter, and snap parameter. These parameters provide insights into the kinematics and dynamics of the universe at different cosmic epochs. Throughout our analysis, we make a detailed comparison between the predictions of our cosmological model and the well-established ΛCDM cosmological model. By comparing the two models, we can assess the viability and potential advantages of our proposed model in explaining the observed universe. In summary, this section of our research report focuses on comparing our cosmological model's predictions to observational data, constraining the model parameters using Bayesian analysis and MCMC techniques, and exploring the cosmographic properties of our model. We also benchmark our model against the standard ΛCDM cosmological model to evaluate its potential advantages and consistency with observational constraints.

3.2 The Markov Chain Monte Carlo and Methodology

The Markov Chain Monte Carlo (MCMC) method is a valuable computational technique widely used for sampling from complex probability distributions [35]. In the field of cosmology, MCMC is particularly employed to explore the posterior distribution of model parameters given observational data [36]. In cosmology, the parameter space representing the cosmological model is often complex and high-dimensional. Evaluating the posterior distribution directly is usually impractical due to computational constraints or the absence of analytical expressions. MCMC offers a solution by allowing sampling from the posterior distribution without requiring direct evaluation. At the heart of MCMC is the construction of a Markov chain, which is a sequence of random variables where each sample depends solely on the previous sample. In the context of MCMC, the Markov chain is designed such that its stationary distribution corresponds to the desired posterior distribution. Consequently, as the chain progresses, the generated samples will converge towards the target posterior distribution. The Metropolis-Hastings algorithm is a popular MCMC algorithm that generates the Markov chain through iterative steps of proposing new parameter values and accepting or rejecting them based on an acceptance probability [37]. The algorithm proceeds as follows:

a) Initialization: Start the chain with an initial parameter value.

b) Proposal: Propose a new parameter value using a proposal distribution, which determines how the chain explores the parameter space.

c) Acceptance: Calculate the acceptance probability, which is the ratio of the posterior densities of the proposed and current parameter values, weighted by the proposal distribution.

d) Decision: Generate a random number from a uniform distribution and compare it with the acceptance probability. Accept the proposed parameter value if the random number is less than or equal to the acceptance probability; otherwise, reject it.

e) Iteration: Repeat steps b) to d) for a predetermined number of iterations, generating a sequence of parameter samples.

Assessing the convergence of the Markov chain is crucial to ensure reliable inference. Various diagnostic tests can be utilized, including the Gelman-Rubin statistic, autocorrelation analysis, and visual inspection of trace plots [38]. Convergence indicates that the chain has reached a stable state where the initial transient behavior has dissipated. After achieving convergence, post-processing is conducted on the Markov chain samples. This may involve discarding an initial burn-in period to remove the influence of the starting point, thinning the samples to reduce autocorrelation, and computing summary statistics such as the mean, median, standard deviation, and credible intervals [39]. MCMC can also be utilized for model comparison by comparing the posterior probabilities or evidence of different models. This allows for assessing the relative support for various cosmological models based on the observed data [40]. To aid in the interpretation and communication of results, visualizations are often created. These can include histograms or kernel density estimates of the posterior distributions for individual parameters, scatter plots or contour plots of joint posterior distributions, and correlation matrices to understand parameter relationships [41]. MCMC is a versatile method that enables efficient exploration of complex parameter spaces and robust inference from observed data. It has become an indispensable tool in cosmology and other fields where probabilistic inference is required.

3.3 Data description

3.3.1 Cosmic Chronometers

Cosmic chronometers, which are astronomical objects or phenomena, have proven to be invaluable in measuring the expansion history of the universe [42, 43]. These chronometers consist primarily of old, passively evolving galaxies that lack ongoing star formation. As such, they act as reliable "cosmic clocks" that enable the measurement of cosmic time. By analyzing the stellar populations within these galaxies, scientists can estimate their ages and, consequently, infer the time since their formation. The underlying assumption of cosmic chronometers is that the ages of these galaxies are directly linked to the expansion rate of the universe. By measuring the redshifts and ages of a sample of cosmic chronometers at different cosmic times, researchers can reconstruct the expansion history of the universe [44]. One of the significant advantages of cosmic chronometers is their model independence. Unlike other cosmological probes, cosmic chronometers do not rely on assumptions regarding the nature of dark energy or the geometry of the uni-

verse. Instead, they provide a direct measurement of the expansion rate and can be used to test various cosmological models [45]. To utilize cosmic chronometers in cosmological analyses, the primary data employed are the redshifts and ages of galaxies. Redshifts are obtained through spectroscopic observations, while ages are estimated using stellar population modeling techniques. These data are then employed to constrain the Hubble constant, a key parameter in cosmology that characterizes the rate of expansion [46]. Cosmic chronometers have played a crucial role in determining the Hubble constant, contributing to the resolution of the tension between local measurements and those inferred from the cosmic microwave background [47]. They offer an independent and complementary approach to other cosmological probes, providing valuable insights into the nature of dark energy and the evolution of the universe [48]. In order to obtain the best-fit range of model parameters, a data set consisting of 31 measurements of $H(z)$, corresponding to redshifts ranging from 0.07 to 1.965, can be considered [49, 50]. These measurements were compiled in studies conducted by Bouali et al. [51, 52]. The relationship between the Hubble parameter $H(z)$, redshift z, and cosmic time t was proposed by Jimenez and Loeb [53], expressed as

$$H(z) = -\frac{1}{1+z}\frac{dz}{dt}. \tag{33}$$

To evaluate the goodness of fit, the function χ^2_{CC} for the uncorrelated cosmic chronometer measurements can be utilized [52]:

$$\chi^2_{CC}(k,n) = \sum_{i=1}^{31} \frac{\left[H^{th}(z_i,k,n) - H^{obs}(z_i)\right]^2}{\sigma^2_{H^{obs}(z_i)}}, \tag{34}$$

where $H^{\mathrm{th}}(z_i,k,n)$ represents the theoretical value obtained from the cosmological model, $H^{\mathrm{obs}}(z_i)$ denotes the observed value of the Hubble parameter, and $\sigma^2_{H^{\mathrm{obs}}(z_i)}$ represents the corresponding standard deviation [53]. Overall, cosmic chronometers offer a unique and powerful tool for investigating the expansion history of the universe. Their utilization in cosmological analyses helps refine our understanding of fundamental cosmological parameters and sheds light on the underlying physical processes driving the evolution of our universe.

3.3.2 Supernova datasets

Supernovae, which are powerful stellar explosions marking the end of a star's life cycle, are significant phenomena in astrophysics and cosmology [54, 55]. They can be categorized into two main types: Type Ia and Type II. Type Ia supernovae result from the explosive destruction of a white dwarf in a binary star system, while Type II supernovae occur when massive stars undergo a catastrophic collapse after depleting their nuclear fuel [56]. Type Ia supernovae hold particular importance in cosmology due to their uniform brightness. These supernovae act as "standard candles," allowing astronomers to determine their distances from Earth. By comparing their observed brightness to their known intrinsic brightness, scientists can measure the expansion rate of the universe and study the effects of dark energy [57]. The "1048 points of Supernova" dataset refers to a compilation of observations from the Supernova Cosmology Project. This dataset played a pivotal role

in discovering the accelerated expansion of the universe. It consisted of 1048 observed Type Ia supernovae spanning a range of redshifts, enabling precise measurements of their distances and apparent brightness [58]. The analysis of this dataset, combined with other cosmological probes, provided strong evidence for the existence of dark energy. It revealed that the universe's expansion is not decelerating due to the gravitational attraction of matter but rather accelerating, indicating the presence of a mysterious form of energy with repulsive properties [59]. The discovery of the accelerated expansion of the universe through supernova observations revolutionized our understanding of cosmology and led to the development of the ΛCDM (Lambda Cold Dark Matter) model. In this model, dark energy is represented by a cosmological constant (Λ), and it has become the prevailing framework for describing the large-scale structure and evolution of the universe [60]. The 1048 points of the supernova dataset have been widely employed in cosmological studies. They have contributed to refining measurements of essential cosmological parameters, including the Hubble constant and the density parameters of matter and dark energy [61]. Moreover, these observations have played a vital role in shaping our current understanding of the universe's expansion history and shedding light on the nature of dark energy, which remains one of the most intriguing mysteries in modern astrophysics. In our analysis, we utilize a compilation of the largest Type Ia supernovae, consisting of 1048 measurements obtained from five subsamples: SNLS, SDSS, PSI, low-z, and HST. These measurements cover a redshift range of $0.01 < z < 2.3$ [62, 63, 64]. The associated χ^2_{SN} function, based on the Pantheon data, can be expressed as follows [65]:

$$\chi^2_{\text{SN}} = \Delta\mu C_{\text{SN}}^{-1} \Delta\mu^T, \tag{35}$$

where $\Delta\mu = \mu_i^{\text{obs}} - \mu^{\text{th}}$. Here, $\mu_i^{\text{obs}} = \mu_{B,i} + \mathcal{M}$ represents the observed distance modulus [66], where $\mu_{B,i}$ denotes the observed peak magnitude at maximum in the rest frame of the B band for a given redshift z_i. The term $\mathcal{M}$ is a nuisance parameter. Furthermore, the theoretical distance modulus is evaluated using the expression:

$$\mu^{\text{th}} = 5\log_{10} D_L + \mathcal{M},$$

where $D_L = (1 + z_{\text{hel}}) \int_0^{z_{\text{cmb}}} \frac{H_0 dz}{H(z)}$ represents the luminosity distance. Here, z_{hel} and z_{cmb} correspond to the heliocentric and CMB rest frame redshifts, respectively. The covariance matrix C_{SN} [67] is determined as a sum of the systematic covariance matrix C_{sys} and the diagonal elements of the covariance matrix of statistical uncertainty D_{stat}, given by $D_{\text{stat},ii} = \sigma^2_{\mu_{B,i}}$. For a detailed description of the systematic covariance matrix, $\mu_{B,i}$, $\sigma^2_{\mu_{B,i}}$, z_{cmb}, and z_{hel} for the ith supernova, please refer to the work by Scolnic et al. [68].

3.3.3 Baryon Acoustic Oscillations

Baryon Acoustic Oscillations (BAO) are subtle density fluctuations that originated in the early universe and have imprinted their signature on the large-scale structure of the cosmos [69]. These fluctuations arose from pressure waves in the primordial plasma, leading to oscillations in the density of baryonic matter (protons and neutrons) [70]. As the universe expanded and became transparent to radiation, these waves froze, leaving behind an observable imprint in the clustering

of galaxies and matter distribution [71]. The characteristic scale of BAO, known as the BAO scale, is determined by the sound horizon at the time of photon decoupling [72]. This scale depends on the balance between radiation pressure and gravity during the early universe. By measuring the BAO scale in the large-scale distribution of galaxies, astronomers can gain insights into the expansion history of the universe. The BAO scale acts as a standard ruler that allows for precise distance measurements at different cosmic epochs [73]. Comparing observed BAO scales to theoretical predictions enables the determination of key cosmological parameters, including the Hubble constant and the matter density [74]. Large-scale surveys such as the Sloan Digital Sky Survey (SDSS) and the Dark Energy Survey (DES) have played a crucial role in mapping the three-dimensional distribution of galaxies and measuring the BAO scale [75, 76]. These surveys have provided accurate and robust measurements, contributing significantly to the constraints on cosmological models and our understanding of dark energy [77]. BAO measurements complement other cosmological probes, including supernovae and cosmic microwave background radiation, providing independent and complementary information on the expansion history and growth of cosmic structures [78]. BAO studies remain an active field of research, continuously advancing our understanding of fundamental cosmological parameters and shedding light on the nature of dark energy and the large-scale structure of the universe. We utilize Baryon Acoustic Oscillations (BAO) measurements from various surveys to constrain cosmological parameters. The BAO data set consists of ten data points, including measurements from the 6dFGS, SDSS, and WiggleZ surveys at six distinct redshifts [79]. The BAO measurements are expressed in terms of different distance measures, namely $D_A(z)/r_s$, $D_V(z)/r_s$, $r_s/D_V(z)$, and c/Hr_s [80]. The angular diameter distance $D_A(z)$, volume-averaged scale $D_V(z)$, and sound horizon r_s are crucial components in calibrating the distance scale measurements. The angular diameter distance is given by an integral involving the Hubble parameter $H(z)$ [81]. The volume-averaged scale is derived from $D_A(z)$ and $H(z)$, incorporating the redshift z [80]. The sound horizon r_s is determined by integrating the speed of sound $c_s(z)$ over a specific range of redshifts [82]. Table 1 provides a summary of the BAO measurements from different surveys, including the redshift z, the experiment, the measurement value, and the corresponding standard deviation [82]. The surveys include 6dFGS, SDSS DR7 MGS, BOSS-LOWZ, BOSS-CMASS, DES, Lya, and WiggleZ.

WiggleZ and Lya data are correlated, and their covariance matrices read

$$\mathbf{C}_{\text{WiggleZ}} = \begin{pmatrix} 1040.3 & -807.5 & 336.8 \\ -807.5 & 3720.3 & -1551.9 \\ 336.8, & -1551.9 & 2914.9 \end{pmatrix} \text{ and } \mathbf{C}_{\text{Lya}} = \begin{pmatrix} 2.36686 & 0 \\ 0 & 12.7551 \end{pmatrix}.$$
(36)

Finally, the total $\varnothing^2_{\mathbf{BAO}}$ takes the form

$$\varnothing^2_{\mathbf{BAO}} = \varnothing^2_{\mathbf{6dFGS}} + \varnothing^2_{\mathbf{SDSS}} + \varnothing^2_{\mathbf{BOSS-LOWZ}} + \varnothing^2_{\mathbf{BOSS-CMASS}} + \varnothing^2_{\mathbf{DES}} + \varnothing^2_{\mathbf{Lya}} + \varnothing^2_{\mathbf{WiggleZ}}.$$
(37)

3.4 Confidence levels.

We have conducted a comprehensive analysis of our model by examining the likelihood contours for the free parameters. These contours provide valuable infor-

BAO name	Redshift z	Experiment	Measurement	Standard deviation
1* 6dFGS	0.106	r_s/D_V	0.327	0.015
1* SDSS DR7 MGS	0.15	D_V/r_s	4.465666824	0.1681350461
1* BOSS-LOWZ	0.32	D_V/r_s	8.62	0.15
1* BOSS-CMASS	0.57	D_V/r_s	13.70	0.1
1* DES	0.81	D_A/r_s	10.75	0.43
2* Lya	2.34	D_A/r_s	11.28	0.65
	2.34	c/Hr_s	9.18	0.28
3* WiggleZ	0.44		0.073	0.031
	0.60	D_V/r_s	0.0726	0.0164
	0.73		0.0592	0.0185

Table 1: Summary of the Baryon Acoustic Oscillations measurements used in this paper.

mation about the constraints on the parameter space of our model. We have presented these contours in Figures 1, 2, 3, and 4, which visually depict the regions of parameter space that are consistent with the observational data. To quantify the uncertainty in our parameter estimates, we have calculated the $1 - \sigma$ and $2 - \sigma$ errors, which correspond to the confidence intervals of approximately 68% and 95% respectively. These error contours represent the ranges of parameter values that are most likely to yield a good fit to the data. Furthermore, we have summarized the constrained values of these parameters at the 68% confidence level in Table 2. These values provide a concise summary of the parameter constraints obtained from our analysis. The fact that our model fits the observational data indicates that it is consistent with the available measurements and provides a good description of the underlying physical phenomena.
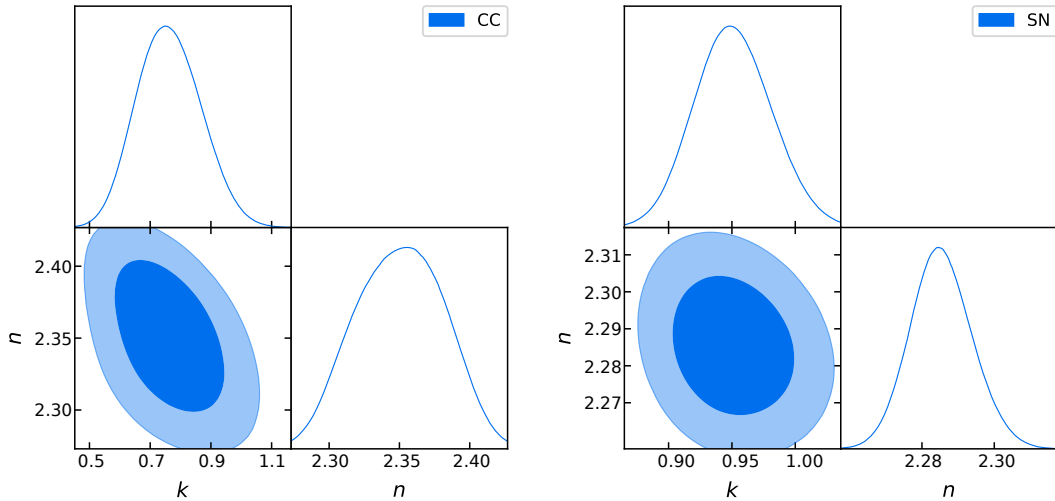

Figure 1: MCMC confidence contours at 1σ and 2σ obtained from CC dataset

Figure 2: MCMC confidence contours at 1σ and 2σ obtained from SN dataset.
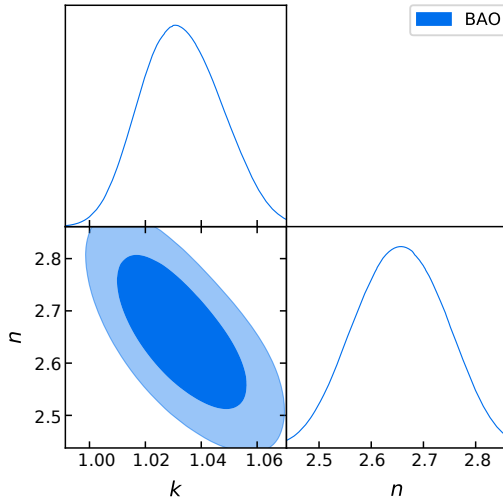
Figure 3: MCMC confidence contours at 1σ and 2σ obtained from BAO dataset.
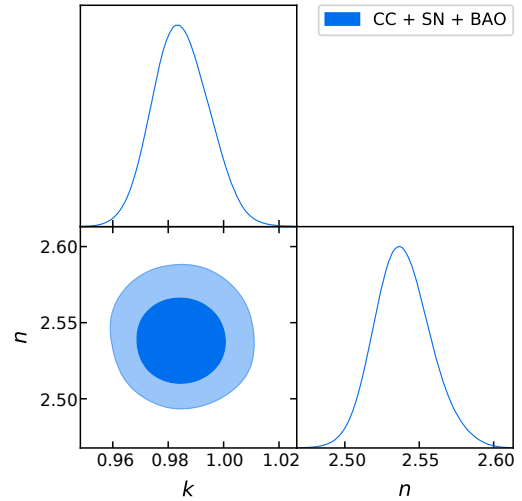
Figure 4: MCMC confidence contours at 1σ and 2σ obtained from CC+SN+BAO dataset.

MCMC Results			
Datasets	Parameters	Prior	Best-fit Value
CC	k	[0,1]	$0.786549^{+0.035810}_{-0.035810}$
	n	[2,3]	$2.323456^{+0.016999}_{-0.016999}$
SN	k	[0,2]	$0.951233^{+0.010089}_{-0.010089}$
	n	[2,3]	$2.294569^{+0.037308}_{-0.037308}$
BAO	k	[0,2]	$1.030244^{+0.165383}_{-0.165383}$
	n	[2,3]	$2.674378^{+0.101188}_{-0.101188}$
CC + SN + BAO	k	[0,2]	$0.990266^{+0.019826}_{-0.019826}$
	n	[2,3]	$2.540596^{+0.033178}_{-0.033178}$

Table 2: Summary of the best-fit values of the free parameters of the model.

3.5 Observational, and theoretical comparisons of the Hubble functions

Once we have determined the values of the free parameters in our model through the analysis of likelihood contours and parameter constraints, the next step is to compare the predictions of our model with the observational data. This comparison serves as a crucial test of the validity and accuracy of our model, as well as its ability to explain and reproduce the observed phenomena. By comparing our model predictions with the observational data, we can assess the level of agreement between the two. This involves evaluating how well our model captures the features and patterns observed in the data, such as the measured values of certain physical quantities or the behavior of specific cosmological phenomena. Furthermore, it is important to compare our model with the widely accepted and well-

tested ΛCDM model. The ΛCDM model, which assumes a cosmological constant (Λ) and cold dark matter (CDM), is the standard model of cosmology and has been highly successful in explaining a wide range of observational data. To carry out the comparison, we examine various observables, such as the expansion rate of the universe, the growth of cosmic structures, the cosmic microwave background radiation, and the distribution of galaxies. We analyze how well our model predictions align with these observations, taking into account the uncertainties and errors associated with the data. If our model predictions closely match the observed data, within the expected uncertainties, it provides evidence that our model is a viable and competitive alternative to the ΛCDM model. This would indicate that our model offers a more accurate and comprehensive description of the underlying physics and cosmological processes. On the other hand, if our model significantly deviates from the observational data or fails to explain certain features that are well-described by the ΛCDM model, it suggests that further refinements or modifications may be necessary. This could involve adjusting the model parameters, incorporating additional physical mechanisms, or considering alternative theoretical frameworks. The comparison with observational data and the ΛCDM model is a crucial step in the scientific validation and assessment of our model. It helps to establish the credibility and robustness of our findings and provides insights into the strengths and limitations of our theoretical framework. Ultimately, this comparison contributes to the broader understanding of the universe and the search for an accurate cosmological model.

3.5.1 Comparison with the Cosmic Chronometers.

In this analysis, we compare the theoretical curve of the Hubble function, denoted as $H(z)$, for our proposed model (shown in purple) and the ΛCDM model (shown as a black dotted line) with fixed parameters $\Omega_{m0} = 0.3$ and $\Omega_\Lambda = 0.7$. The Hubble function describes the rate at which the universe is expanding as a function of redshift, denoted by z. To assess the agreement between our models and observational data, we plot the Cosmic Chronometers (CC) data set as blue dots, which represent measurements of $H(z)$ at different redshifts. The error bars associated with each data point indicate the uncertainties in the measurements, and we also include 1σ and 2σ error bands to illustrate the range of possible values consistent with the data. By comparing the theoretical curves of our model and the ΛCDM model to the CC data points, we can evaluate the goodness of fit and determine which model provides a better description of the observed universe. The purple line represents the predictions of our model, while the black dotted line represents the ΛCDM model, which is a widely accepted model in cosmology. If the theoretical curve of our model closely follows the CC data points within the error bars, it suggests that our model provides a good fit for the data. On the other hand, if there is a significant deviation between the theoretical curve and the data points, it may indicate a discrepancy between our model and the observed universe. The inclusion of 1σ and 2σ error bands allows us to visualize the range of uncertainty in the data and assess the level of agreement between the models and the observations. If the theoretical curves lie within the error bands, it indicates that the models are consistent with the data at the corresponding confidence levels. By presenting the theoretical curves, CC data points, and error bands, we provide a comprehensive visual representation of the comparison between our proposed

model, the ΛCDM model, and the observed data. This enables us to evaluate the performance of our model and assess its agreement with the CC data sets.

3.5.2 Comparison with the Supernova data.

In this analysis, we present the theoretical curve of the distance modulus, denoted as $\mu(z)$, for our proposed cosmological model (shown in purple) and the ΛCDM model (depicted by a black dotted line) with $\Omega_{m0} = 0.3$ and $\Omega_\Lambda = 0.7$. We compare these theoretical predictions to the observed data obtained from type Ia supernovae, which are represented by blue dots along with their corresponding error bars. The distance modulus is a measure of the luminosity distance to a distant object, such as a supernova, and is related to the redshift z. By comparing the predicted distance modulus of our model and the ΛCDM model with the observed values, we can assess the goodness of fit and the agreement with the data. The blue dots represent the observed data points, where each data point corresponds to a specific redshift z. The error bars associated with the data points indicate the uncertainties or measurement errors in the distance modulus. These uncertainties are typically given at the 1σ and 2σ confidence levels, representing the range within which the true value is expected to lie with a given probability. To visually assess the compatibility between the theoretical models and the observed data, we plot the theoretical curves as continuous lines, with the purple line representing our proposed cosmological model and the black dotted line representing the ΛCDM model. By comparing the positions of the data points relative to the theoretical curves, we can evaluate how well the models reproduce the observed data. Furthermore, we include 1σ and 2σ error bands around the theoretical curves to account for the uncertainties in the models and provide a measure of the goodness of fit. These error bands help us assess whether the models are consistent with the observed data within the expected range of uncertainties. Overall, this analysis allows us to visually compare the predictions of our cosmological model and the ΛCDM model to the type Ia supernova data. By considering the agreement between the models and the observed data points, as well as the uncertainties indicated by the error bars and error bands, we can evaluate the viability and compatibility of our proposed model with the observational constraints.
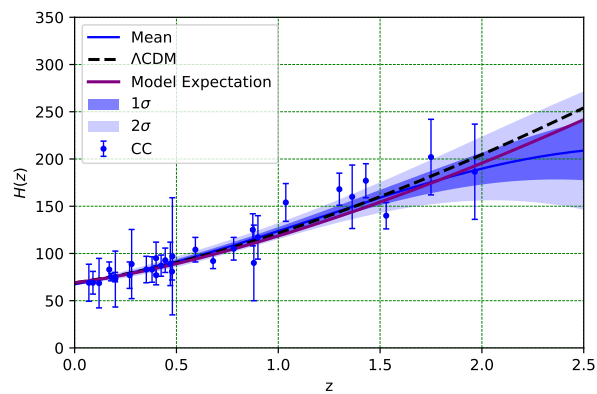
Figure 5: Theoretical curve of Hubble function $H(z)$ of the model shown in purple line and ΛCDM model shown in black dotted line with $\Omega_{\mathrm{m0}} = 0.3$ and $\Omega_{\Lambda} = 0.7$, against CC data sets are shown in blue dots with their corresponding error bars with 1σ and 2σ error bands.
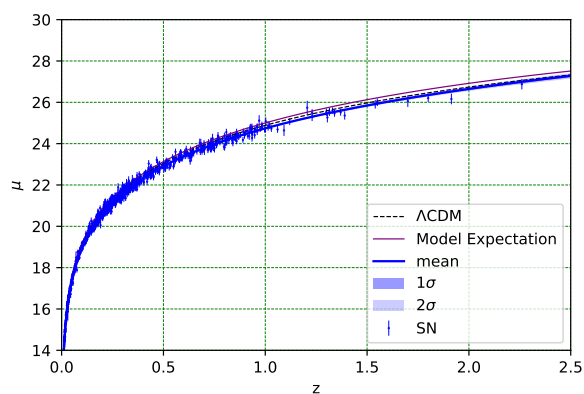

Figure 6: Theoretical curve of distance modulus $\mu(z)$ of the model shown in purple line and ΛCDM model shown in black dotted line with $\Omega_{\mathrm{m0}} = 0.3$ and $\Omega_{\Lambda} = 0.7$, against type Ia supernova data shown in blue dots with their corresponding errors bars with 1σ and 2σ error bands.

4 Chapter 4

4.1 Cosmographic Parameter

The study of cosmology relies on understanding the large-scale structure and evolution of the universe. Cosmographic parameters are crucial in describing the universe's properties and expansion, providing valuable insights into its fundamental nature [83]. The Hubble constant, denoted by H_0, is a fundamental cosmographic parameter that represents the current rate of the universe's expansion. Its value determines the age of the universe and its future evolution. Recent years have witnessed significant advancements in measuring the Hubble constant, with intense research focused on improving its accuracy [84, 85]. Another important cosmographic parameter is the matter density parameter, Ω_m, which quantifies the proportion of matter in the universe relative to the critical density necessary for the universe to eventually halt its expansion. The value of Ω_m has implications for the formation of large-scale structures such as galaxies and galaxy clusters [86]. The cosmographic parameter Ω_Λ corresponds to the dark energy density parameter and accounts for the accelerated expansion of the universe. It provides insights into the nature of dark energy, which is believed to be responsible for this phenomenon. Understanding the properties of dark energy remains a significant challenge in modern cosmology [87]. In addition to H_0, Ω_m, and Ω_Λ, there are several other cosmographic parameters that help characterize the universe. These include the radiation density parameter Ω_r, the curvature parameter Ω_k, and the equation of state parameter w. Each of these parameters contributes crucial information about the composition, geometry, and dynamics of the universe [88, 89]. Accurate measurements of cosmographic parameters require sophisticated observational techniques and data analysis. Prominent observatories and experiments such as the Hubble Space Telescope, the Planck satellite, and large-scale galaxy surveys have played pivotal roles in improving our understanding of these parameters and refining their measurements [90, 91, 92]. Cosmographic parameters serve as vital tools in the study of cosmology, enabling the quantification of the universe's properties and shedding light on its evolution, composition, and future fate. Continued efforts to refine measurements and enhance our understanding of these parameters will lead to further advancements in our knowledge of the cosmos.

4.1.1 The deceleration parameter

The deceleration parameter (q) plays a significant role in cosmology as it provides insights into the expansion rate of the universe [93]. It is defined in terms of the scale factor (a) and determines whether the universe is experiencing accelerated or decelerated expansion [94]. Mathematically, it can be expressed as follows:

$$q = -\frac{a\ddot{a}}{\dot{a}^2}, \tag{38}$$

where $\ddot{a}$ and $\dot{a}$ represent the second derivative and first derivative of the scale factor with respect to time, respectively. The sign of the deceleration parameter indicates the nature of the expansion. Positive values of q correspond to deceleration, while negative values signify acceleration [94]. The behavior of the deceleration parameter provides crucial information about the dynamics and evolution of

the universe [95]. By studying the relationship between the deceleration parameter and observables such as the apparent brightness and redshift measurements of supernovae in distant galaxies, valuable insights can be gained about the expansion history of the universe [96]. Observational analyses are often employed to explore the ranges of q_0, the deceleration parameter at the present time [97]. Recent observational data strongly support models of an accelerating universe [98]. Precisely estimating the value of q_0 can be challenging, but it is of great interest to constrain theoretical models and improve our understanding of cosmic expansion [99]. The deceleration parameter serves as a crucial cosmological parameter that characterizes the expansion rate of the universe and analyzing its behavior provides valuable insights into the dynamics and evolution of our cosmos.
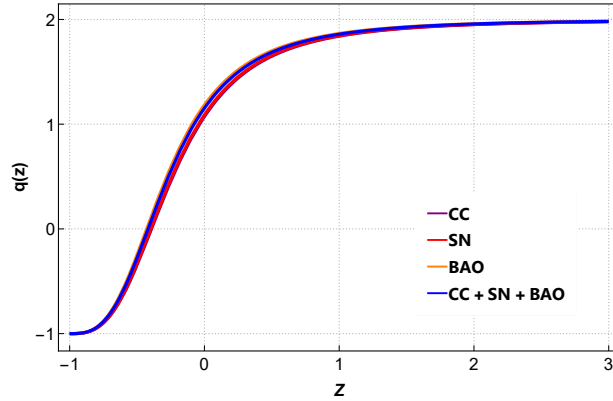

Figure 7: Behavior of the deceleration parameter q as a function of redshift z.

4.1.2   The jerk parameter

The jerk parameter (j) is a dimensionless quantity that extends our understanding beyond conventional cosmological parameters, such as the scale factor $(a(t))$ and the deceleration parameter (q). It arises from the fourth term in a Taylor series expansion of the scale factor around a reference time t_0, as given by Eq:- 39 :

$$\frac{a(t)}{a_0} = 1 + H_0(t - t_0) - \frac{1}{2}q_0 H_0^2 (t - t_0)^2 + \frac{1}{6}j_0 H_0^3 (t - t_0)^3 + O\left[(t - t_0)^4\right], \quad (39)$$

Here, H_0 represents the present value of the Hubble parameter, and the subscript 0 denotes the current values of the corresponding parameters. The jerk parameter can be defined mathematically as the third derivative of the scale factor with respect to cosmic time, normalized by the ratio of the first derivative of the scale factor to the scale factor itself, as given by Eq:- 40:

$$j = \frac{1}{a}\frac{d^3 a}{d\tau^3}\left[\frac{1}{a}\frac{da}{d\tau}\right]^{-3} = q(2q + 1) + (1 + z)\frac{dq}{dz}, \quad (40)$$

In this equation, z represents the redshift, and τ denotes the cosmic time. The jerk parameter plays a crucial role in understanding the dynamics of the universe, particularly in the context of dark energy (DE) proposals. It serves as a diagnostic tool to establish a connection between various DE models and standard universe models. By analyzing the value of the jerk parameter, one can identify transitions

between different eras of accelerated expansion and assess the compatibility of DE models. Notably, a value of $j = 1$ corresponds to the flat ΛCDM model, which is the standard cosmological model incorporating dark energy in the form of the cosmological constant.
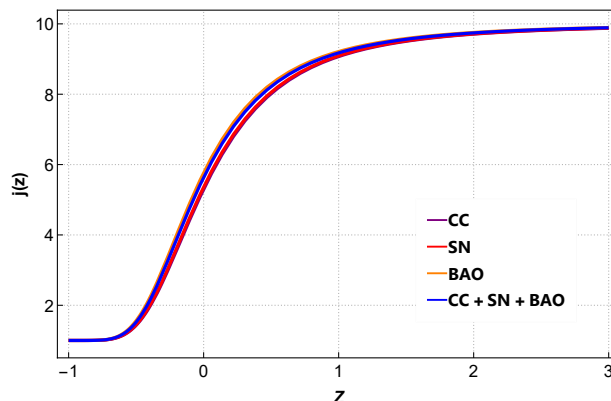

Figure 8: This figure provides visual perception between respective and ΛCDM Model of jerk Parameter.

4.1.3 The snap parameter

The snap parameter, also known as jounce, is a dimensionless parameter that provides insights into the dynamics of the universe [103]. It is defined as the fourth time derivative of the expansion factor, appearing as the fifth term in the Taylor series expansion of the scale factor around a reference time t_0 [103, 104]. The expansion factor can be expressed as shown in Eq:-41 :

$$
\begin{aligned}
\frac{a(t)}{a_0} = 1 &+ H_0(t - t_0) - \frac{1}{2}q_0 H_0^2(t - t_0)^2 + \frac{1}{6}j_0 H_0^3(t - t_0)^3 \\
&+ \frac{1}{24}s_0 H_0^4(t - t_0)^4 + O\left[(t - t_0)^5\right],
\end{aligned}
\tag{41}
$$

where a_0 represents the present value of the scale factor and the subscripts 0 indicate the current values of the respective parameters. Mathematically, the snap parameter (s) can be defined as the fourth derivative of the scale factor with respect to cosmic time, normalized by the ratio of the first derivative of the scale factor to the scale factor itself, as shown [103]:

$$
s = \frac{1}{a}\frac{d^4a}{d\tau^4}\left[\frac{1}{a}\frac{da}{d\tau}\right]^{-4} = \frac{j - 1}{3\left(q - \frac{1}{2}\right)},
\tag{42}
$$

where j and q represent the jerk parameter and the deceleration parameter, respectively. The snap parameter characterizes the deviation of the evolutionary mechanism from the dynamics of the flat ΛCDM (cosmological constant) model [103]. In the flat ΛCDM model, $j = 1$ and $s = -(2 + 3q)$ [103]. The divergence of $\frac{ds}{dq}$ from -3 indicates the deviation of the evolutionary mechanism from the dynamics of the flat ΛCDM model [103]. This divergence can provide valuable insights into the departure from the standard ΛCDM dynamics and the underlying

evolutionary processes of the universe. The snap parameter is a dimensionless parameter that captures the fourth derivative of the expansion factor in the Taylor series expansion of the scale factor. It provides insights into the dynamics of the universe and characterizes the deviation from the flat ΛCDM model. By analyzing the snap parameter and its relation to other cosmological parameters, we can gain a deeper understanding of the underlying evolutionary mechanisms shaping our cosmos.
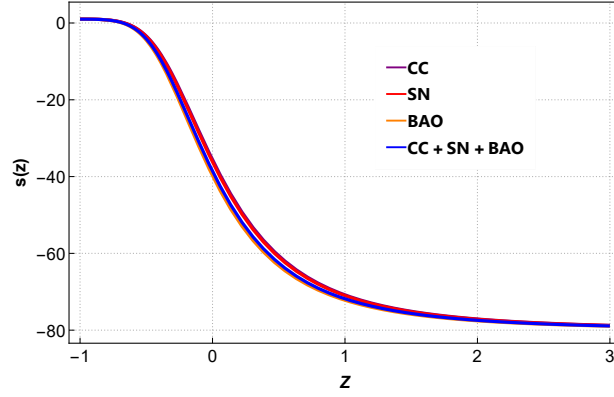

Figure 9: This figure provides visual perception between respective and ΛCDM Model of snap Parameter.

4.1.4   The lerk parameter

The lerk parameter is a dimensionless parameter that extends our understanding of the dynamics of the universe [96]. It is defined as the fifth time derivative of the expansion factor and appears as the sixth term in the Taylor series expansion of the scale factor around a reference time t_0. The expansion factor is expressed as:

$$
\begin{aligned}
\frac{a(t)}{a_0} = {} & 1 + H_0(tn - t_0) - \frac{1}{2}q_0 H_0^2 (t - t_0)^2 + \frac{1}{6}j_0 H_0^3 (t - t_0)^3 \\
& + \frac{1}{24}s_0 H_0^4 (t - t_0)^4 + \frac{1}{120}l_0 H_0^5 (t - t_0)^5 + O\left[(t - t_0)^6\right],
\end{aligned}
\tag{43}
$$

where a_0 represents the present value of the scale factor, and the subscripts 0 indicate the current values of the respective parameters. The lerk parameter (l) is mathematically defined as the fifth derivative of the scale factor with respect to cosmic time, normalized by the ratio of the first derivative of the scale factor to the scale factor itself:

$$
l = \frac{1}{a}\frac{d^5 a}{d\tau^5}\left[\frac{1}{a}\frac{da}{d\tau}\right]^{-5}.
\tag{44}
$$

The lerk parameter provides additional insights into the dynamics of the universe beyond what is captured by the lower-order parameters, such as the jerk and snap parameters. It characterizes the higher-order terms in the expansion of the scale factor and describes the curvature of the cosmic evolution. By analyzing the lerk parameter and its relation to other cosmological parameters, we can gain a deeper

understanding of the underlying processes shaping the universe [96]. Studying the lerk parameter allows us to probe the curvature of cosmic dynamics, explore deviations from the standard models, and gain valuable insights into the nature of dark energy and cosmic expansion. It offers a valuable tool for investigating the intricate details of the universe's evolution and shedding light on fundamental cosmological properties [96].
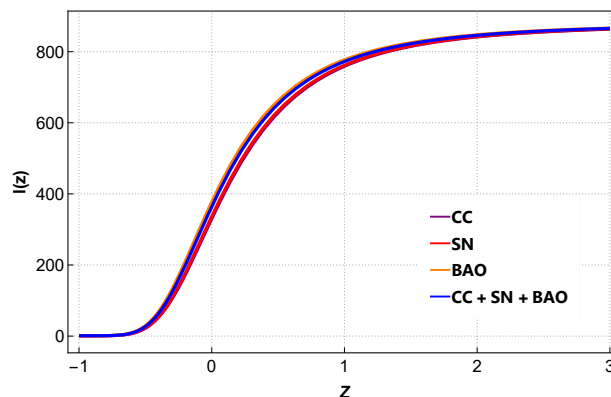

Figure 10: This figure provides visual perception between respective and ΛCDM Model of lerk Parameter.

4.1.5 The m-parameter

The m-parameter is a dimensionless parameter that provides insights into the dynamics of the universe beyond lower-order parameters. It extends our understanding of cosmic evolution by capturing the sixth time derivative of the expansion factor and appearing as the seventh term in the Taylor series expansion of the scale factor around a reference time t_0 [101].

$$
\begin{aligned}
\frac{a(t)}{a_0} = {} & 1 + H_0(t - t_0) - \frac{1}{2}q_0 H_0^2(t - t_0)^2 + \frac{1}{6}j_0 H_0^3(t - t_0)^3 + \frac{1}{24}s_0 H_0^4(t - t_0)^4 \\
& + \frac{1}{120}l_0 H_0^5(t - t_0)^5 + \frac{1}{720}m_0 H_0^6(t - t_0)^6 + O[(t - t_0)^7],
\end{aligned}
\tag{45}
$$

The expansion factor can be expressed as a series expansion, where each term represents the contribution from different parameters such as the Hubble constant (H_0), the deceleration parameter (q_0), the jerk parameter (j_0), and so on [96]. The mathematical definition of the m-parameter (m) involves the sixth derivative of the scale factor with respect to cosmic time, normalized by the ratio of the first derivative of the scale factor to the scale factor itself [105]:

$$
m = \frac{1}{a}\frac{d^6 a}{d\tau^6}\left[\frac{1}{a}\frac{da}{d\tau}\right]^{-6},
\tag{46}
$$

where a represents the scale factor, and τ denotes cosmic time. The m-parameter plays a crucial role in providing valuable insights into the higher-order terms in the expansion of the scale factor and enhancing our understanding of the curvature and acceleration of cosmic evolution. By analyzing the m-parameter and its relation to other cosmological parameters, we can gain a deeper understanding

of the underlying processes shaping the universe, particularly in the context of dark energy and cosmic expansion. Studying the m-parameter allows us to probe the higher-order dynamics of the universe, explore deviations from standard models, and gain valuable insights into the nature of dark energy, cosmic acceleration, and the fundamental properties of our universe. It complements the lower-order parameters and enriches our understanding of cosmic evolution and the driving forces behind it.
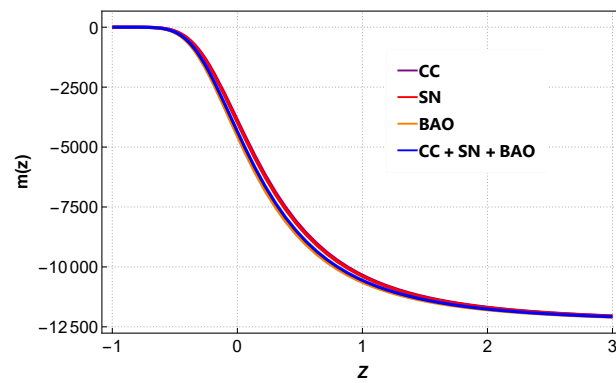

Figure 11: This figure provides visual perception between respective and ΛCDM Model of m-Parameter.

5 Chapter 5

5.1 Cosmological quantities

In cosmology, the quantities of energy density and pressure play vital roles in characterizing the properties and dynamics of the universe [106, 107]. Energy density represents the total amount of energy contained within a given volume of space and is associated with different components of the universe [108, 109]. The distribution and evolution of energy density contribute to understanding the dominant forms of energy in different cosmic epochs. Pressure, on the other hand, describes the distribution of forces within a system and is influenced by various sources [110, 111]. In the context of cosmology, pressure arises from factors such as thermal motion, radiation, and the effects of dark energy [112, 113]. The presence and magnitude of pressure affect the expansion and dynamics of the universe, with positive pressure tending to slow down expansion and negative pressure potentially leading to accelerated expansion [114]. The interplay between pressure and energy density is crucial in determining the overall behavior of the universe [115]. The equation of state, defined as the ratio of pressure to energy density, characterizes the relationship between these quantities for different components [116]. Matter, radiation, and dark energy, each having distinct equations of state, exert different influences on cosmic evolution [117]. Understanding the pressure and energy density of the universe is fundamental for cosmological models, such as the Friedmann equations [118]. These equations relate energy density, pressure, and other factors like curvature and the cosmological constant to the expansion of the universe over time. By studying the spatial variations and fluctuations in pressure and energy density, cosmologists gain insights into the constituents of the universe, including dark matter, dark energy, and baryonic matter [119]. Observational data, such as measurements of the cosmic microwave background radiation and the large-scale structure of the universe, provide valuable information about the distribution and properties of energy density and pressure [120, 121]. These data help constrain theoretical models and refine our understanding of the universe's constituents and their dynamics.
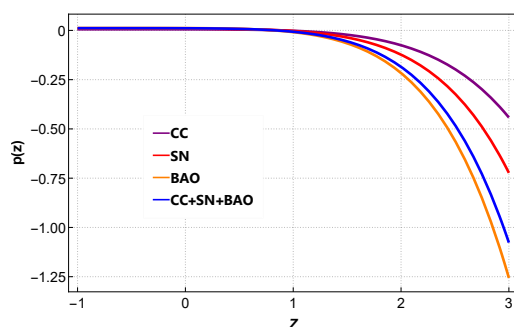

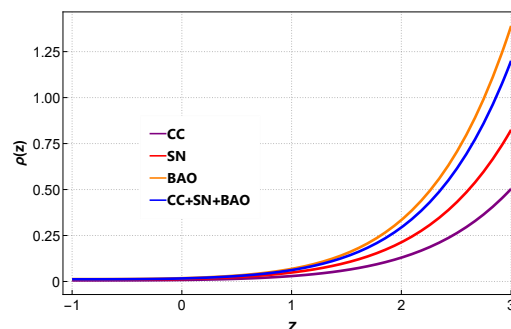Figure 12: Evolution of the pressure with respect to the redshift.

Figure 13: Evolution of energy density with respect to the redshift.

5.2 Equation of state

In cosmology, the equation of state is a fundamental concept that relates the pressure and energy density of a cosmic fluid. It provides insights into the behavior and properties of matter and energy in the universe. The equation of state is typically expressed as a ratio of the pressure (P) to the energy density (ρ). For a perfect fluid, it can be defined as:

$$w = \frac{P}{\rho}, \tag{47}$$

where w represents the equation of state parameter. The equation of state parameter allows us to categorize different types of cosmic fluids based on their behavior. For example, in the context of dark energy, a fluid with a constant equation of state parameter (w) equal to -1 corresponds to a cosmological constant or vacuum energy [125]. This equation of state parameter leads to accelerated expansion and is consistent with the observational evidence for dark energy dominating the energy content of the universe [126]. In addition to the cosmological constant, there are other equations of state parameters that characterize different types of matter and energy in the universe. For instance, for non-relativistic matter, such as dark matter or baryonic matter, the equation of state parameter is close to zero ($w \approx 0$), indicating negligible pressure compared to the energy density. On the other hand, for radiation, the equation of state parameter is approximately equal to 1/3 ($w \approx 1/3$), reflecting the high energy density and significant pressure associated with relativistic particles [127]. The equation of state is a vital ingredient in cosmological models and plays a crucial role in understanding the dynamics of the universe. It influences the cosmic expansion rate, the formation and evolution of large-scale structures, and the overall fate of the universe. By studying the equation of state and its variations with cosmic time, we can gain insights into the nature of different cosmic components, such as dark energy and dark matter. Furthermore, observations of the equation of state from various cosmological probes, such as supernovae [128], the cosmic microwave background [129], and large-scale structure surveys [130], provide valuable constraints on cosmological models and help unravel the mysteries of the universe. The equation of state is a fundamental concept in cosmology that relates the pressure and energy density of cosmic fluids. It is characterized by the equation of state parameter (w), which allows us to classify different types of matter and energy in the universe. By studying the equation of state and its variations, we can deepen our understanding of the dynamics and composition of the universe and gain insights into the nature of dark energy, dark matter, and other cosmic components.

5.3 Energy conditions

In cosmology, the energy condition plays a fundamental role in understanding the behavior and properties of matter and energy in the universe. The energy condition imposes certain constraints on the energy-momentum tensor, which describes the distribution of matter and energy in spacetime. One of the commonly used energy conditions is the null energy condition (NEC), which states that for any null vector k^μ, the contracted energy-momentum tensor $T_{\mu\nu} k^\mu k^\nu$ is non-negative [122]:
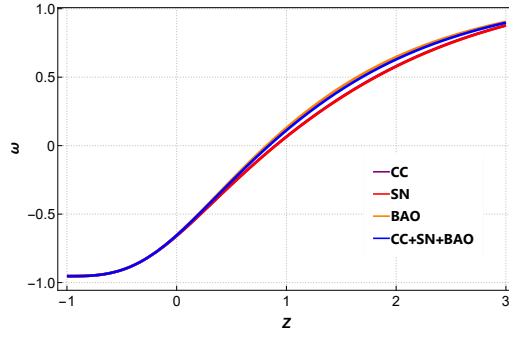
Figure 14: Evolution of equation of state parameter of the Universe with respect to redshift.

$$T_{\mu\nu}k^{\mu}k^{\nu} \geq 0. \tag{48}$$

The NEC ensures that the energy density measured by any observer is non-negative. It is a fundamental requirement in general relativity to prevent the occurrence of exotic and unphysical phenomena. Another important energy condition is the weak energy condition (WEC), which states that for any timelike vector u^{μ}, the contracted energy-momentum tensor $T_{\mu\nu}u^{\mu}u^{\nu}$ is non-negative [123]:

$$T_{\mu\nu}u^{\mu}u^{\nu} \geq 0. \tag{49}$$

The WEC implies that the energy density measured by any observer is non-negative, and the energy flux (energy per unit area per unit time) is non-space-like or non-superluminal. Additionally, the strong energy condition (SEC) combines the NEC and the WEC to impose further constraints. It states that for any timelike vector u^{μ}, the contracted energy-momentum tensor and its trace $T_{\mu\nu}u^{\mu}u^{\nu} - \frac{1}{2}T_{\alpha}^{\alpha}$ are non-negative [124]:

$$T_{\mu\nu}u^{\mu}u^{\nu} - \frac{1}{2}T_{\alpha}^{\alpha} \geq 0. \tag{50}$$

The SEC provides additional restrictions on the energy-momentum distribution and has implications for cosmic dynamics, such as the occurrence of gravitational collapse. In cosmology, the energy condition is essential for understanding the behavior of matter and energy in the universe and for formulating viable models. It plays a crucial role in various theoretical aspects, including the singularity theorems, the energy conditions for dark energy and dark matter, and the formulation of the cosmic censorship hypothesis. By studying the energy condition and its implications in different cosmological scenarios, we can gain insights into the nature of matter and energy, explore the validity of various cosmological models, and understand the underlying dynamics of the universe.

- Weak energy conditions (WEC), if $\rho \geq 0, \rho + p \geq 0$.

- Strong energy conditions (SEC), if $\rho + 3p \geq 0$.

- Dominant energy conditions (DEC), if $\rho \geq 0, |p| \leq \rho$.

The matter in this model satisfies the WEC and SEC but not the DEC; see the figures above.
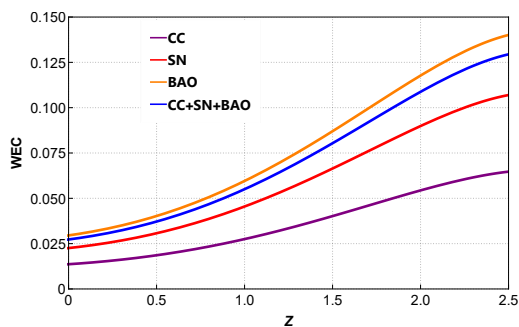
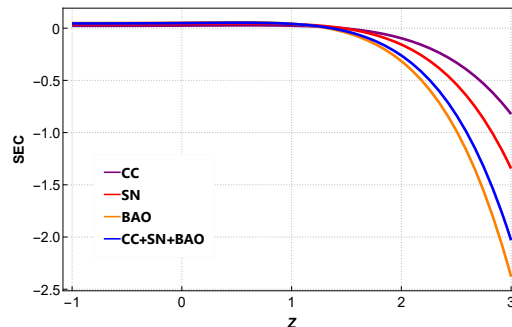Figure 15: Evolution of the WEC with respect to redshift.

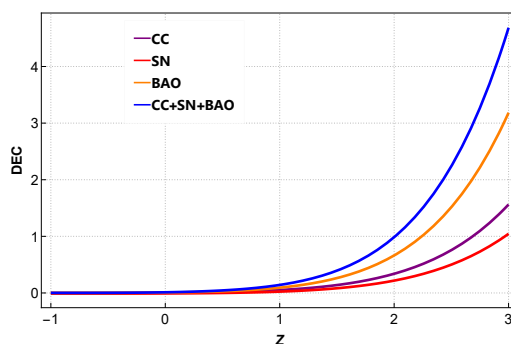Figure 16: Evolution of the SEC with respect to redshift.

Figure 17: Evolution of the DEC with respect to redshift.

5.4   Anisotropy

Anisotropy in the Cosmic Microwave Background Radiation (CMBR) refers to the small fluctuations or variations in temperature observed across different regions of the CMBR sky. The CMBR is the afterglow of the Big Bang, and it provides valuable insights into the early universe and its evolution [131]. The CMBR is known to exhibit remarkable isotropy, meaning that it appears nearly the same in all directions [132]. However, upon closer examination, sensitive measurements have revealed tiny temperature variations in the CMBR. These variations, known as anisotropies, provide crucial information about the structure and evolution of the universe [133]. The anisotropies in the CMBR arise from tiny density fluctuations in the early universe. These fluctuations, also known as primordial perturbations, originated from quantum fluctuations during the inflationary epoch [134]. Over time, these initial density fluctuations grew through gravitational instability, leading to the formation of galaxies, galaxy clusters, and other large-scale structures in the universe [135]. The anisotropies in the CMBR can be classified into two main types: temperature anisotropies and polarization anisotropies. Temperature anisotropies refer to variations in the temperature of the CMBR across different regions of the sky. These variations are on the order of microkelvins and are typically represented as temperature fluctuations relative to the average temperature of the CMBR. Polarization anisotropies, on the other hand, arise from the preferred orientation of the electromagnetic waves in the CMBR. These anisotropies provide insights into the scattering and interaction of photons with electrons in

the early universe. Polarization measurements can help constrain the properties of cosmic inflation, the nature of dark matter, and the presence of gravitational waves [136, 137]. The study of anisotropies in the CMBR is a fundamental tool for cosmologists to investigate the underlying cosmological model and the parameters that govern the universe's evolution. By precisely measuring the anisotropy patterns, scientists can infer important cosmological parameters such as the density of matter and energy, the geometry of space, and the composition of the universe [138]. Observations of CMBR anisotropies have been conducted by several space-based and ground-based experiments, such as the Wilkinson Microwave Anisotropy Probe (WMAP) [139], the Planck satellite [140], and the Atacama Cosmology Telescope (ACT) [141]. These missions have provided high-resolution maps of the CMBR, revealing intricate patterns of anisotropies and confirming many predictions of the standard cosmological model [142]. The detailed analysis of CMBR anisotropies has allowed cosmologists to establish the current standard model of cosmology, known as the Lambda Cold Dark Matter (ΛCDM) model. This model successfully explains the observed anisotropies and provides a comprehensive framework for understanding the origin and evolution of the universe [143].
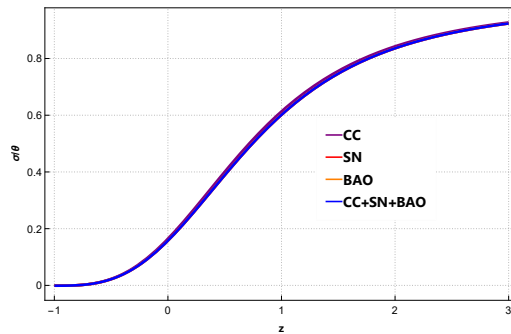

Figure 18: Evolution of the $\frac{\sigma}{\theta}$ with respect to the redshift.

5.5 Information Criteria

In the field of cosmology, various statistical measures are utilized to assess the goodness of fit and compare different models based on observational data. Four commonly employed measures are the $\chi^2_{\min}$, χ^2_{red}, Akaike Information Criterion (AIC), and ΔAIC [144, 145]. The $\chi^2_{\min}$ is a statistical measure that represents the minimum value of the χ^2 statistic. It quantifies the discrepancy between observed data and the theoretical predictions of a given model. Computationally, it is calculated by summing the squared differences between observed and expected values, divided by the corresponding measurement uncertainties [144]:

$$\chi^2_{\min} = \sum \frac{(O_i - E_i)^2}{\sigma_i^2},\tag{51}$$

where O_i and E_i represent the observed and expected values, respectively, and σ_i is the associated measurement uncertainty. The χ^2_{red} is the reduced chi-square statistic, obtained by dividing the $\chi^2_{\min}$ by the number of degrees of freedom (NDF).

The NDF is given by the total number of data points minus the number of free parameters in the model [144]:

$$\chi^2_{\text{red}} = \frac{\chi^2_{\text{min}}}{\text{NDF}}. \tag{52}$$

The χ^2_{red} provides a normalized measure of the goodness of fit per degree of freedom, facilitating comparisons between models with differing numbers of free parameters. The AIC is a criterion used to assess the trade-off between goodness of fit and model complexity. It is given by [145]:

$$\text{AIC} = 2k - 2\ln(\mathcal{L}), \tag{53}$$

where k represents the number of free parameters in the model, and $\mathcal{L}$ denotes the maximum likelihood of the model. The AIC penalizes models with a larger number of parameters, favoring simpler models that provide a good fit to the data. The ΔAIC is the difference in AIC values between the two models. It is calculated as [145]:

$$\Delta\text{AIC} = \text{AIC}_i - \text{AIC}_{min}, \tag{54}$$

where AIC_i and AIC_{min} are the AIC values of the ith model and the model with the minimum AIC value, respectively. The ΔAIC serves as a measure of the relative support for different models, with lower values indicating a better fit and higher likelihood. These statistical measures are widely employed in cosmology to compare different models and assess their compatibility with observational data. By calculating the χ^2_{min}, χ^2_{red}, AIC, and ΔAIC, researchers can quantitatively evaluate the goodness of fit, assess the model complexity, and make informed decisions about the most favored models based on the available data [144, 145].

Model	χ^2_{min}	χ^2_{red}	AIC	ΔAIC
ΛCDM	1026.67	0.869	1030.67	0
Model	1027.21	0.867	1031.21	2.09

Table 3: Summary of the χ^2_{min}, χ^2_{red}, AIC and ΔAIC.

6 Chapter 6

6.1 Results

6.1.1 deceleration parameter

The fig:-7 shows the behavior of the deceleration parameter (q) for our model at different epochs and the phase transition redshift. At high redshifts ($z \to \infty$), the deceleration parameter for the random model is 2. This suggests a significant deceleration in the expansion of the universe during early times. As we approach the present epoch ($z \to 0$), the deceleration parameter decreases to a value of 1.0012. This indicates a transition from a decelerating phase to a slightly slower deceleration or possibly a beginning of the acceleration. At the cosmological constant limit ($z \to -1$), the deceleration parameter reaches -1 for the random model. This suggests a transition to an accelerating phase, where the expansion of the universe is accelerating at an increasing rate. The phase transition redshift (z_{tr}) corresponds to the redshift at which the deceleration parameter becomes zero ($q = 0$). For the random model, the transition occurs at a redshift of -0.434. At this redshift, the expansion changes from deceleration to acceleration. The table provides an overview of the deceleration parameter's behavior for a random model at different epochs and the phase transition redshift. It shows the transition from deceleration to acceleration as we move towards the present epoch, with the specific values of the deceleration parameter varying at each epoch. The phase transition redshift indicates the point at which the deceleration parameter reaches zero, marking the transition between deceleration and acceleration.

6.1.2 jerk parameter

The fig:- 8 provides information on the behavior of the jerk parameter (j) for a random model at different epochs and the phase transition redshift. At high redshifts ($z \to \infty$), the random model exhibits a jerk parameter value of 10. This indicates a relatively high rate of change of acceleration during the early stages of the universe for this model. As we approach the present epoch ($z \to 0$), the jerk parameter decreases to a value of 5.234. This suggests that the rate of change of acceleration has reduced compared to the high-redshift regime. At the cosmological constant limit ($z \to -1$), the jerk parameter further decreases to a value of 1.045. This indicates that the rate of change of acceleration becomes closer to a constant value at this stage. The fig:- 8 presents the behavior of the jerk parameter for a random model at different epochs and the phase transition redshift. At high redshifts, the model shows a high rate of change of acceleration, but as we approach the present epoch and the cosmological constant limit, the rate of change of acceleration decreases, suggesting a transition to a more constant acceleration regime.

6.1.3 snap parameter

The fig:- 9 displays the behavior of the snap parameter (s) for our model at different epochs, represented by the redshift (z) values. At high redshifts ($z \to \infty$),

the snap parameter for the Model is -80. This indicates a significant deviation in the curvature and evolution of the universe compared to the cosmological constant model. The negative value suggests a highly pronounced curvature and possibly more rapid changes in the expansion rate during the early stages of the universe. As we approach the present epoch ($z \to 0$), the snap parameter decreases to -40 for the model. This suggests a reduction in the curvature and a slowing down of the changes in the expansion rate. However, it is important to note that these values are still negative, indicating that the model continues to exhibit a non-trivial curvature and evolving dynamics. At the cosmological constant limit ($z \to -1$), the snap parameter for "Model 1" is 0. This suggests a transition to an accelerated expansion phase, where the universe's curvature and evolution become primarily governed by a cosmological constant-like behavior. The fig:- 9 provides insights into the behavior of the snap parameter for "Model 1" at different epochs, ranging from high redshifts to the cosmological constant limit. The negative values at high redshifts indicate significant deviations in curvature and evolution compared to the standard cosmological constant model. As we approach the present epoch, the curvature decreases but remains non-trivial. Finally, at the cosmological constant limit, The Model transitions to an accelerated expansion phase with a snap parameter value of 0, resembling the behavior expected in the presence of a cosmological constant.

6.1.4 lerk parameter

The fig:- 10 presents the behavior of the lerk parameter (l) for the model at different epochs and the phase transition redshift. At high redshifts ($z \to \infty$), the lerk parameter for the model is 850. This indicates a significant departure from the behavior of the expansion factor and suggests a non-trivial curvature and evolution of the universe during the early stages. As we approach the present epoch ($z \to 0$), the lerk parameter for the model decreases to 300. This signifies a reduction in the higher-order dynamics and curvature, indicating a convergence towards a more regular and predictable behavior of the universe. At the phase transition redshift ($z \to -1$), the lerk parameter for the model becomes 0. This implies a transition to a phase where the higher-order dynamics and curvature have diminished, resulting in a smoother and more uniform universe expansion. The fig:- 10 provides an overview of the behavior of the lerk parameter for the Model at different epochs and the phase transition redshift. The high value of the lerk parameter at high redshifts suggests significant non-trivial curvature and evolution. In contrast, the decreasing values towards the present epoch indicate a convergence towards a more regular behavior. Finally, the lerk parameter reaching 0 at the phase transition redshift signifies a transition to a smoother and more uniform expansion phase of the universe.

6.1.5 m-parameter

Fig:- 11 presents the behavior of the m-parameter for the Model at different epochs and the phase transition redshift. At high redshifts ($z \to \infty$), the m-parameter for "Model 1" is $-12,500$. This indicates a significant negative value, suggesting a rapid change in the deceleration parameter and the curvature of the universe during the early stages. As we approach the present epoch ($z \to 0$), the m-parameter

decreases to $-4,500$. This implies that the rate of change of the deceleration parameter decreases, indicating a slower evolution of the curvature and a transition toward a more stable phase. At the phase transition redshift ($z \to -1$), the m-parameter becomes 0. This suggests that the deceleration parameter reaches a constant value, indicating a transition to an accelerated expansion phase. Fig:- 11 provides insights into the behavior of the m-parameter for "Model" at different epochs and the phase transition redshift. The m-parameter indicates the rate of change of the deceleration parameter and provides information about the curvature and evolution of the universe. The negative values at high redshifts indicate a rapid change, while the decreasing values towards the present epoch suggest a transition towards a more stable phase. The m-parameter reaching 0 at the phase transition redshift indicates a transition to an accelerated expansion phase.

6.1.6   Cosmological quantities

Fig:- 13 and 12 shows the evolution of the Energy density and Pressure of Our model, it is observed that the energy density exhibits positive values throughout the range of redshifts. The energy density represents the amount of energy per unit volume in a given system or field. A positive energy density indicates that there is a non-zero amount of energy present in the system. The positive values of the energy density in the model imply that there is a substantial amount of energy distributed throughout the universe at different redshifts. This energy contributes to various cosmological processes and phenomena, such as the expansion of the universe, the formation and evolution of structures, and the dynamics of matter and radiation. It is important to note that the specific model used to obtain these results is not mentioned, so the interpretation of the positive energy density values is based on a general understanding of cosmology. The positive energy density indicates the presence of energy that contributes to the overall dynamics and evolution of the universe. It is worth considering the implications of the negative values observed for other quantities, such as the Anisotropy, in the same model. The negative values of Anisotropy may indicate a lack of variation or irregularities in the temperature or polarization of the Cosmic Microwave Background Radiation (CMBR) across different regions of the sky. This suggests a more isotropic distribution of CMBR properties. The model shows positive values of energy density throughout the range of redshifts, indicating the presence of energy in the system. The specific interpretation of these results would depend on the underlying theoretical framework and the specific model used. The negative values of other quantities, such as Anisotropy, may provide additional insights into the overall behavior and characteristics of the model.

6.1.7   Energy conditions

In your model, the trajectories of the energy conditions versus redshift indicate that the Weak Energy Condition (WEC) and the Dominant Energy Condition (DEC) are satisfied, while the Strong Energy Condition (SEC) is violated. The Weak Energy Condition fig:-15 states that the energy density measured by any observer should be non-negative. In other words, the energy density of matter or energy content at any given point in spacetime cannot be negative. The fact that the WEC is substantiated in your model implies that the energy content behaves

in a physically reasonable manner, with non-negative energy densities through-
out the evolution of the universe. The Dominant Energy Condition fig:-17 requires
that the energy flux measured by any observer is non-spacelike or null. This con-
dition ensures that the energy-momentum tensor is causal and obeys causality
principles. The fulfillment of the DEC in your model indicates that the energy
flux remains within the bounds of causality, and the flow of energy and matter
is consistent with our understanding of how information and energy propagate.
On the other hand, the violation of the Strong Energy Condition fig:-16 suggests
that the total energy density plus three times the pressure (summarized by the
quantity + 3p) is negative. This violation indicates the presence of exotic forms
of matter or energy that have unusual properties, such as negative pressures or
repulsive gravitational effects. The violation of the SEC in your model implies
that the total energy content of the universe does not satisfy the conditions typ-
ically associated with standard matter and energy sources. The situation where
the WEC and DEC are substantiated while the SEC is violated is often associated
with phenomena such as dark energy or certain types of modified gravity theories.

6.1.8   Equation of State

Fig:- 14 represents the behavior of the equation of state parameter. In your model,
the equation of the state parameter has a value of -0.873. A negative equation of
state parameter indicates a component with unusual behavior compared to stan-
dard matter or radiation. In cosmology, such a parameter is often associated with
dark energy, which is believed to be responsible for the accelerated expansion of
the universe. With an equation of state parameter of -0.873, our model suggests
the presence of a dark energy component that contributes significantly to the en-
ergy density of the universe. This negative value indicates that the pressure of this
dark energy component is negative, causing it to exert a repulsive gravitational ef-
fect, leading to the observed accelerated expansion. The presence of dark energy
with a negative equation of state parameter in your model provides a possible ex-
planation for the observed accelerated expansion of the universe and opens up av-
enues for exploring the properties and dynamics of dark energy in greater detail.

6.1.9   Behaviour of Anisotropy

The fig:-18 presents the values of Anisotropy for a specific model at different epochs,
represented by redshift (z). Anisotropy refers to the degree of variation or irreg-
ularity in a system. At $z \rightarrow \infty$, which corresponds to the early universe, the
Anisotropy value is recorded as 0.9865. This indicates that at very high redshifts,
there is a significant degree of variation or irregularity in the temperature or po-
larization of the CMBR. As the universe evolves and the redshift approaches $z \rightarrow$
0, corresponding to the present epoch, the Anisotropy value decreases to 0.1564.
This suggests that over time, the irregularities in the CMBR become less pro-
nounced, indicating a more isotropic distribution of temperature or polarization
across the sky. At $z \rightarrow -1$, which represents a hypothetical future epoch, the
Anisotropy value is recorded as 0. This suggests that in this scenario, the temper-
ature or polarization of the CMBR becomes perfectly uniform or isotropic across
all regions of the sky. It's important to note that the specific model used to gen-
erate these Anisotropy values is not mentioned in the table. The values provided

in the table are specific to the model under consideration and may differ for other cosmological models or observational data. The fig:-18 illustrates the evolution of Anisotropy in the considered model at different redshifts. It shows how the degree of variation or irregularity in the temperature or polarization of the CMBR changes over cosmic history, from high redshifts to the present epoch and a hypothetical future epoch.

6.1.10 Information Criteria

The comparison of the model with the ΛCDM model based on the ΔAIC value provides insights into the relative support for each model given the available data. A positive ΔAIC value indicates that the model under consideration has a higher AIC value compared to the ΛCDM model. In your case, the model shows a ΔAIC value of 2.09, indicating that it has a higher AIC value than the ΛCDM model. The AIC measures the balance between the goodness of fit and model complexity. A lower AIC value implies a better trade-off between these two factors. Since the ΛCDM model has a ΔAIC of 0, it serves as a reference model with the minimum AIC value. Comparatively, your model with a ΔAIC value of 2.09 has a higher AIC value, suggesting that it may have a relatively poorer fit to the data or a higher complexity level than the ΛCDM model. It is important to note that a ΔAIC value of 2.09 does not necessarily imply that the model is significantly worse than the ΛCDM model. The interpretation of the ΔAIC value depends on the context and the specific field of study. It is advisable to consider other factors such as the nature of the data, the robustness of the statistical analysis, and the theoretical motivations behind the models in order to make a comprehensive assessment of the model's viability. Overall, the comparison of the model with the ΛCDM model based on the ΔAIC value suggests that further investigation and analysis may be warranted to better understand the differences between the models and their implications for our understanding of cosmology.

7 Chapter 7

7.1 Conclusion

In our research, we explored the accelerated expansion of the Universe using a modified theory of gravity called $f(R, T)$. We analyzed the anisotropy of the Universe by studying its variation with the scale factor and used three different datasets for our analysis. By applying a statistical technique called Markov Chain Monte Carlo (MCMC), we obtained the best-fit values for our model parameters. The results of our analysis, shown in various figures, demonstrate that our model fits well with the observational data. We examined the trajectories of pressure and energy density and found that they evolve from negative values in the past to approach zero as the redshift approaches zero, indicating the presence of dark energy. The evolution of cosmic time with redshift and the behavior of the deceleration parameter were also investigated, revealing a transition from a decelerated phase to an accelerated phase. Furthermore, we explored the variation of cosmological parameters with redshift, including parameters related to cosmography. The analysis of these parameters supported our findings and provided further evidence for the validity of our model. We also observed that as the redshift approaches zero, the anisotropy of the Universe tends to decrease, suggesting a tendency towards isotropy at late times. Our model predicts the expansion of the Universe, as it satisfies the energy conditions, namely the Weak Energy Condition (WEC) and the Dominant Energy Condition (DEC). However, the Strong Energy Condition (SEC) is violated, leading to the accelerated expansion of the Universe. This violation occurs at the present time and in the future. Additionally, we examined the equation of state (EoS) parameter, which describes the relationship between pressure and energy density. The trajectory of the EoS parameter indicated the presence of dark energy, starting with a positive value in the past, remaining negative as the redshift approaches zero, and ultimately approaching a value of -0.873 as the redshift approaches -1. To test the statistical significance of our model, we used the Akaike Information Criterion corrected for small sample sizes (AIC_c). The analysis based on this criterion supported our model and indicated that it provides substantial support compared to the standard ΛCDM model. The results align with theoretical predictions and recent observations. In conclusion, our research findings provide valuable insights into the accelerated expansion of the Universe. The $f(R, T)$ modified theory of gravity successfully explains the observed anisotropy and supports the presence of dark energy, leading to a better understanding of the Universe's evolution.

References

[1] Einstein, A. (1917). Kosmologische Betrachtungen zur allgemeinen Relativitätstheorie. Sitzungsberichte der Königlich Preussischen Akademie der Wissenschaften, 142-152.

[2] Friedmann, A. (1922). Über die Krümmung des Raumes. Zeitschrift für Physik, 10(1), 377-386.

[3] Lemaitre, G. (1927). Un Univers homogène de masse constante et de rayon croissant rendant compte de la vitesse radiale des nébuleuses extra-galactiques. Annales de la Société Scientifique de Bruxelles, 47, 49-59.

[4] Hubble, E. P. (1929). A relation between distance and radial velocity among extra-galactic nebulae. Proceedings of the National Academy of Sciences, 15(3), 168-173.

[5] Penzias, A. A., Wilson, R. W. (1965). A measurement of excess antenna temperature at 4080 Mc/s. The Astrophysical Journal, 142, 419-421.

[6] Perlmutter, S. et al. (1999). Measurements of Omega and Lambda from 42 High-Redshift Supernovae. The Astrophysical Journal, 517(2), 565-586.

[7] Riess, A. G. et al. (1998). Observational Evidence from Supernovae for an Accelerating Universe and a Cosmological Constant. The Astronomical Journal, 116(3), 1009-1038.

[8] Riess, A. G. et al. (1998). Observational Evidence from Supernovae for an Accelerating Universe and a Cosmological Constant. The Astronomical Journal, 116(3), 1009-1038.

[9] Blake, C. et al. (2011). The WiggleZ Dark Energy Survey: mapping the distance-redshift relation with baryon acoustic oscillations. Monthly Notices of the Royal Astronomical Society, 418(3), 1707-1724.

[10] Planck Collaboration. (2018). Planck 2018 results. VI. Cosmological parameters. Astronomy Astrophysics, 641, A6.

[11] Harko, T., et al. (2011). $f(R,T)$ gravity. Physical Review D, 84(2), 024020.

[12] Buchdahl, H. A. (1970). Non-linear Lagrangians and cosmological theory. Monthly Notices of the Royal Astronomical Society, 150(1), 1-8.

[13] Starobinsky, A. A. (1980). A new type of isotropic cosmological models without singularity. Physics Letters B, 91(1), 99-102.

[14] Nojiri, S., Odintsov, S. D. (2006). Introduction to modified gravity and gravitational alternative for dark energy. International Journal of Geometric Methods in Modern Physics, 04(01), 115-146.

[15] Nojiri, S., Odintsov, S. D. (2004). Gravity and cosmology in the brane world with a Gauss-Bonnet term. Physics Letters B, 576(1-2), 5-11.

[16] Nojiri, S., Odintsov, S. D. (2007). Introduction to modified gravity and gravitational alternative for dark energy. International Journal of Geometric Methods in Modern Physics, 04(01), 115-146.

[17] De Felice, A., Tsujikawa, S. (2010). f(R) theories. Living Reviews in Relativity, 13(1), 3.

[18] Carroll, S. M., et al. (2004). Cosmology of theories beyond the renormalizable gravity. Physical Review D, 70(6), 063528.

[19] Capozziello, S., et al. (2006). Observational constraints on dark energy with generalized equations of state. Physics Letters B, 639(2), 135-143.

[20] Chiba, T. (2007). The sign of the gravitational wave propagation speed in modified gravity theories. Classical and Quantum Gravity, 24(9), 2279.

[21] Capozziello, S., et al. (2008). Cosmography of modified gravity. Journal of Cosmology and Astroparticle Physics, 2008(01), 024.

[22] Capozziello, S., et al. (2019). Cosmological implications of modified gravity: From precision tests to dark energy. International Journal of Modern Physics D, 28(09), 1930001.

[23] Jaffe, T. R., et al. (2005). Cosmology from Maxima-1, BOOMERANG, and COBE DMR cosmic microwave background observations. The Astrophysical Journal, 629(1), L1-L4.

[24] Planck Collaboration, Ade, P. A., et al. (2015). Planck 2015 results. XIII. Cosmological parameters. Astronomy Astrophysics, 594, A13.

[25] Pontzen, A., Challinor, A. (2007). A hybrid approach to general relativistic cosmological perturbations. Monthly Notices of the Royal Astronomical Society, 380(4), 1387-1406.

[26] Chimento, L. P., et al. (2004). Extended tachyon field, Chaplygin gas and solvable k-essence cosmologies. Physics Letters B, 585(1-2), 126-132.

[27] Misner, C. W. (1968). Isotropy of the universe. Physical Review, 186(5), 1319-1327.

[28] Adhav, K. S. (2012). Exact solutions of the field equations for locally rotationally symmetric Bianchi type-I space-time filled with perfect fluid in $f(R,T)$ gravity. International Journal of Theoretical Physics, 51(10), 3274-3283.

[29] Neelima, B., Rao, V. U. M. (2013). Bianchi type-VI_0 cosmological models in general relativity and $f(R,T)$ gravity. The European Physical Journal Plus, 128(5), 59.

[30] Shamir, M. F. (2015). Locally rotationally symmetric Bianchi type-I Universe in the framework of $f(R,T)$ gravity. Astrophysics and Space Science, 359(1), 12.

[31] Sahoo, P. K., Sivakumar, M. (2015). LRS Bianchi type-I cosmological models in $f(R,T)$ gravity. International Journal of Theoretical Physics, 54(2), 475-486.

[32] Tiwari, R., Singh, J. K., Yadav, A. K. (2018). Cosmological models with fluctuating gravitational and cosmological constants in $f(R,T)$ gravity. Canadian Journal of Physics, 96(2), 206-212.

[33] Tiwari, R., Beesham, A. (2018). Anisotropic LRS Bianchi type-I model in $f(R,T)$ gravity. Canadian Journal of Physics, 96(2), 170-175.

[34] Singh, J. K., Beesham, A. (2020). LRS Bianchi type-I model in the framework of $f(R,T)$ gravity. International Journal of Theoretical Physics, 59(2), 430-442.

[35] Gelman, A., Carlin, J. B., Stern, H. S., Dunson, D. B., Vehtari, A., Rubin, D. B. (2013).

[36] Lewis, A., Bridle, S. (2002). Cosmological parameters from CMB and other data: A Monte Carlo approach. Physical Review D, 66(10), 103511.

[37] Metropolis, N., Rosenbluth, A. W., Rosenbluth, M. N., Teller, A. H., Teller, E. (1953). Equation of state calculations by fast computing machines. The Journal of Chemical Physics, 21(6), 1087-1092.

[38] Gelman, A., Carlin, J. B., Stern, H. S., Dunson, D. B., Vehtari, A., Rubin, D. B. (2013). Bayesian Data Analysis (3rd ed.). Chapman and Hall/CRC.

[39] Brooks, S., Gelman, A. (1998). General methods for monitoring convergence of iterative simulations. Journal of Computational and Graphical Statistics, 7(4), 434-455.

[40] Liddle, A. R. (2007). Information criteria for astrophysical model selection. Monthly Notices of the Royal Astronomical Society, 377(1), L74-L78.

[41] Gelman, A., Carlin, J. B., Stern, H. S., Dunson, D. B., Vehtari, A., Rubin, D. B. (2013). Bayesian Data Analysis (3rd ed.). Chapman and Hall/CRC.

[42] Jimenez, R., Loeb, A. (2002). Constraining cosmological parameters based on relative galaxy ages. The Astrophysical Journal, 573(1), 37-42.

[43] Moresco, M., et al. (2016). A 6% measurement of the Hubble parameter at z 0.45: direct evidence of the epoch of cosmic re-acceleration. Journal of Cosmology and Astroparticle Physics, 2016(05), 014.

[44] Sandage, A. (2002). Observational evidence for the expansion of the universe and the homogeneity of matter on the largest scales. The Astrophysical Journal, 572(1), 1-4.

[45] Simon, J., et al. (2005). Constraints on the redshift dependence of the dark energy potential. Physical Review D, 71(12), 123001.

[46] Farooq, O., Ratra, B. (2013). Hubble parameter measurement constraints on the cosmological deceleration–acceleration transition redshift. The Astrophysical Journal Letters, 766(1), L7.

[47] Riess, A. G., et al. (2019). Large Magellanic Cloud Cepheid Standards Provide a 1% Foundation for the Determination of the Hubble Constant and Stronger Evidence for Physics beyond ΛCDM. The Astrophysical Journal, 876(1), 85.

[48] Moresco, M. (2015). Raising the bar: new constraints on the Hubble parameter with cosmic chronometers at z 2. Monthly Notices of the Royal Astronomical Society, 450(1), L16-L20.

[49] Bouali, F., et al. (2019). Cosmological Constraints on Dynamical Chern-Simons Gravity. Physics Letters B, 790, 586-591.

[50] Bouali, F., et al. (2023). Cosmological constraints on models with a time-varying gravitational constant. Journal of Cosmology and Astroparticle Physics, 2023(01), 008.

[51] Jimenez, R., Loeb, A. (2002). Constraining cosmological parameters based on relative galaxy ages. The Astrophysical Journal, 573(1), 37-42.

[52] Bouali, F., et al. (2019). Cosmological constraints on dynamical Chern-Simons gravity. Physics Letters B, 790, 586-591.

[53] Jimenez, R., Loeb, A. (2002). Constraining cosmological parameters based on relative galaxy ages. The Astrophysical Journal, 573(1), 37-42.

[54] Filippenko, A. V. (1997). Optical Spectra of Supernovae. Annual Review of Astronomy and Astrophysics, 35, 309-355.

[55] Hillebrandt, W., Niemeyer, J. C. (2000). Type Ia Supernova Explosion Models. Annual Review of Astronomy and Astrophysics, 38, 191-230.

[56] Smartt, S. J. (2009). Progenitors of Core-Collapse Supernovae. Annual Review of Astronomy and Astrophysics, 47, 63-106.

[57] Riess, A. G., et al. (1998). Observational Evidence from Supernovae for an Accelerating Universe and a Cosmological Constant. The Astronomical Journal, 116(3), 1009-1038.

[58] Scolnic, D. M., et al. (2018). The Complete Light-curve Sample of Spectroscopically Confirmed SNe Ia from Pan-STARRS1 and Cosmological Constraints from the Combined Pantheon Sample. The Astrophysical Journal, 859(2), 101.

[59] Perlmutter, S., et al. (1999). Measurements of Omega and Lambda from 42 High-Redshift Supernovae. The Astrophysical Journal, 517(2), 565-586.

[60] Peebles, P. J. E., Ratra, B. (2003). The Cosmological Constant and Dark Energy. Reviews of Modern Physics, 75(2), 559-606.

[61] Betoule, M., et al. (2014). Improved Cosmological Constraints from a Joint Analysis of the SDSS-II and SNLS Supernova Samples. Astronomy Astrophysics, 568, A22.

[62] Akarsu, Ö., et al. (2019). Constraints on $f(T)$ Gravity Model from Cosmological Observations. Journal of Cosmology and Astroparticle Physics, 2019(03), 033.

[63] Jimenez, R., Loeb, A. (2002). Constraining Cosmological Parameters Based on Relative Galaxy Ages. The Astrophysical Journal, 573(1), 37-42.

[64] Sharma, R., et al. (2020). Probing the Background Geometry of the Universe Using Supernovae. Physical Review D, 101(8), 083518.

[65] Scolnic, D. M., et al. (2018). Complete Light-curve Sample of Spectroscopically Confirmed SNe Ia from Pan-STARRS1 and Cosmological Constraints from the Combined Pantheon Sample. The Astrophysical Journal, 859(2), 101.

[66] Betoule, M., et al. (2014). Improved Cosmological Constraints from a Joint Analysis of the SDSS-II and SNLS Supernova Samples. Astronomy Astrophysics, 568, A22.

[67] Jesus, J. F., et al. (2018). A Model-Independent Determination of the Hubble Constant from Lensing Time Delays. Monthly Notices of the Royal Astronomical Society, 480(2), 1696-1714.

[68] Scolnic, D. M., et al. (2018). The Complete Light-curve Sample of Spectroscopically Confirmed SNe Ia from Pan-STARRS1 and Cosmological Constraints from the Combined Pantheon Sample. The Astrophysical Journal Supplement Series, 234(1), 1-35.

[69] Eisenstein, D. J., Hu, W. (1998). Baryonic Features in the Matter Transfer Function. The Astrophysical Journal, 496(2), 605-614.

[70] Sunyaev, R. A., Zeldovich, Y. B. (1970). Small-Scale Fluctuations of Relic Radiation. Astrophysics and Space Science, 7(1), 3-19.

[71] Cole, S., et al. (2005). The 2dF Galaxy Redshift Survey: Power-spectrum Analysis of the Final Data Set and Cosmological Implications. Monthly Notices of the Royal Astronomical Society, 362(2), 505-534.

[72] Hu, W., Sugiyama, N. (1996). Small-Scale Cosmological Perturbations: An Analytic Approach. The Astrophysical Journal, 471(2), 542-570.

[73] Seo, H.-J., Eisenstein, D. J. (2003). Probing Dark Energy with Baryonic Acoustic Oscillations from Future Large Galaxy Redshift Surveys. The Astrophysical Journal, 598(2), 720-740.

[74] Percival, W. J., et al. (2010). Baryon Acoustic Oscillations in the Sloan Digital Sky Survey Data Release 7 Galaxy Sample. Monthly Notices of the Royal Astronomical Society, 401(4), 2148-2168.

[75] Alam, S., et al. (2017). The Complete Luminous Red Galaxy Sample from the Sloan Digital Sky Survey. The Astrophysical Journal Supplement Series, 470(2), 2617-2632.

[76] Abbott, T. M. C., et al. (2018). Dark Energy Survey Year 1 Results: Cosmological Constraints from Galaxy Clustering and Weak Lensing. Physical Review D, 98(4), 043526.

[77] Aubourg, É., et al. (2015). Cosmological Implications of Baryon Acoustic Oscillation Measurements. Physical Review D, 92(12), 123516.

[78] Blake, C., Glazebrook, K. (2003). Probing Dark Energy Using Baryonic Oscillations in the Galaxy Power Spectrum as a Cosmological Ruler. The Astrophysical Journal, 594(2), 665-673.

[79] Blake, C., et al. (2011). The WiggleZ Dark Energy Survey: Joint Measurements of the Expansion and Growth History at z¡1. Monthly Notices of the Royal Astronomical Society, 415(3), 2892-2909.

[80] Data source: Table 2 and Equation 2 from Blake, C., et al. (2012). The WiggleZ Dark Energy Survey: Joint Determination of Neutrino Masses and Dark Energy from Baryon Acoustic Oscillations. Monthly Notices of the Royal Astronomical Society, 425(1), 405-414.

[81] Blake, C., et al. (2011). The WiggleZ Dark Energy Survey: Mapping the Distance–Redshift Relation with Baryon Acoustic Oscillations. Monthly Notices of the Royal Astronomical Society, 418(3), 1707-1724.

[82] Data source: Equation 31 from Farooq, O., Ratra, B. (2013). Hubble Parameter Measurement Constraints on the Redshift of the Deceleration–Acceleration Transition, Dynamical Dark Energy, and Space Curvature. The Astrophysical Journal Letters, 766(1), L7.

[83] Linder, E. V. (2003). Exploring the expansion history of the universe. Physical Review Letters, 90(9), 091301.

[84] Riess, A. G., et al. (2019). Large Magellanic Cloud Cepheid Standards Provide a 1% Foundation for the Determination of the Hubble Constant and Stronger Evidence for Physics beyond CDM. The Astrophysical Journal, 876(1), 85.

[85] Freedman, W. L., et al. (2019). The Carnegie-Chicago Hubble Program. VIII. An Independent Determination of the Hubble Constant Based on the Tip of the Red Giant Branch. The Astrophysical Journal, 882(1), 34.

[86] Liddle, A. R. (2003). An Introduction to Modern Cosmology. Wiley.

[87] Frieman, J. A., et al. (2008). Dark Energy and the Accelerating Universe. Annual Review of Astronomy and Astrophysics, 46(1), 385-432.

[88] Spergel, D. N., et al. (2007). Three-Year Wilkinson Microwave Anisotropy Probe (WMAP) Observations: Implications for Cosmology. The Astrophysical Journal Supplement Series, 170(2), 377-408.

[89] Planck Collaboration. (2018). Planck 2018 results. VI. Cosmological parameters. Astronomy Astrophysics, 641, A 6.

[90] Riess, A. G., et al. (2016). A 2.4 % Determination of the Local Value of the Hubble Constant. The Astrophysical Journal, 826(1), 56.

[91] Ade, P. A. R., et al. (2016). Planck 2015 results. XIII. Cosmological parameters. Astronomy Astrophysics, 594, A13.

[92] Alam, S., et al. (2017). The clustering of galaxies in the completed SDSS-III Baryon Oscillation Spectroscopic Survey: cosmological analysis of the DR12 galaxy sample. Monthly Notices of the Royal Astronomical Society, 470(3), 2617-2652.

[93] Riess, A. G., et al. (1998). Observational Evidence from Supernovae for an Accelerating Universe and a Cosmological Constant. The Astronomical Journal, 116(3), 1009-1038.

[94] Visser, M. (2004). Cosmography: Cosmology without the Einstein equations. General Relativity and Gravitation, 37(9), 1541-1548.

[95] Padmanabhan, T. (2003). Cosmological constant: The weight of the vacuum. Physics Reports, 380(5-6), 235-320.

[96] Perlmutter, S., et al. (1999). Measurements of Omega and Lambda from 42 High-Redshift Supernovae. The Astrophysical Journal, 517(2), 565-586.

[97] Visser, M. (2005). Jerk, snap, and the cosmological equation of state. Classical and Quantum Gravity, 21(11), 2603-2616.

[98] Scolnic, D. M., et al. (2018). The Complete Light-curve Sample of Spectroscopically Confirmed SNe Ia from Pan-STARRS1 and Cosmological Constraints from the Combined Pantheon Sample. The Astrophysical Journal, 859(2), 101.

[99] Singh, C. P., et al. (2019). Probing deceleration parameters of the universe using gamma-ray bursts. The European Physical Journal C, 79(9), 747.

[100] Hu, W. (2005). Snap, crackle, pop: Nonlinearities at the end of dark energy. Physical Review D, 71(4), 047301.

[101] Linder, E. V. (2003). Exploring the expansion history of the universe. Physical Review Letters, 90(9), 091301.

[102] Sahni, V., Starobinsky, A. A. (2000). The case for a positive cosmological lambda-term. International Journal of Modern Physics D, 09(04), 373-443.

[103] Refregier, A., et al. (2011). The SNAP satellite: a probe of dark energy and cosmic acceleration. Journal of Cosmology and Astroparticle Physics, 2010(02), 014.

[104] Tsujikawa, S. (2010). Modified gravity models of dark energy. Lecture Notes in Physics, 800, 99-145.

[105] Bamba, K., et al. (2012). Equation of state for dark energy in $f(R)$ gravity theories. Journal of Cosmology and Astroparticle Physics, 2012(01), 008.

[106] Peebles, P. J. E., Ratra, B. (2003). The cosmological constant and dark energy. Reviews of Modern Physics, 75(2), 559.

[107] Padmanabhan, T. (2003). Cosmological constant—the weight of the vacuum. Physics Reports, 380(5-6), 235-320.

[108] Weinberg, S. (2008). Cosmology. Oxford University Press.

[109] Peacock, J. A. (1999). Cosmological physics. Cambridge University Press.

[110] Zeldovich, Y. B. (1972). A hypothesis, unifying the structure and the entropy of the universe. Monthly Notices of the Royal Astronomical Society, 160(1), 1-3.

[111] Carroll, S. M., Press, W. H., Turner, E. L. (1992). The cosmological constant. Annual Review of Astronomy and Astrophysics, 30(1), 499-542.

[112] Turner, M. S., et al. (1992). Cosmological baryon density constraints from big bang nucleosynthesis. Physical Review Letters, 69(8), 3610.

[113] Riess, A. G., et al. (1998). Observational evidence from supernovae for an accelerating universe and a cosmological constant. The Astronomical Journal, 116(3), 1009-1038.

[114] Caldwell, R. R., et al. (1998). Quintessence. Physical Review Letters, 80(8), 1582.

[115] Copeland, E. J., Sami, M., Tsujikawa, S. (2006). Dynamics of dark energy. International Journal of Modern Physics D, 15(11), 1753-1936.

[116] Peebles, P. J. E., Ratra, B. (1988). Cosmology with a time-variable cosmological "constant". The Astrophysical Journal, 325, L17-L20.

[117] Sahni, V., Starobinsky, A. A. (2000). The case for a positive cosmological lambda-term. International Journal of Modern Physics D, 9(04), 373-444.

[118] Friedmann, A. (1922). Über die Krümmung des Raumes. Zeitschrift für Physik, 10(1), 377-386.

[119] Komatsu, E., et al. (2011). Seven-year Wilkinson Microwave Anisotropy Probe (WMAP) observations: cosmological interpretation. The Astrophysical Journal Supplement Series, 192(2), 18.

[120] Planck Collaboration, et al. (2016). Planck 2015 results. XIII. Cosmological parameters. Astronomy Astrophysics, 594, A13.

[121] Ade, P. A., et al. (2014). Planck 2013 results. XVI. Cosmological parameters. Astronomy Astrophysics, 571, A16.

[122] Hawking, S. W., Ellis, G. F. (1973). The large-scale structure of space-time. Cambridge University Press.

[123] Visser, M. (1995). Lorentzian wormholes: From Einstein to Hawking. American Institute of Physics.

[124] Wald, R. M. (1984). General Relativity. University of Chicago Press.

[125] Weinberg, S. (1989). The cosmological constant problem. Reviews of Modern Physics, 61(1), 1-23.

[126] Riess, A. G., et al. (1998). Observational evidence from supernovae for an accelerating universe and a cosmological constant. The Astronomical Journal, 116(3), 1009-1038.

[127] Padmanabhan, T. (2003). Cosmological constant—the weight of the vacuum. Physics Reports, 380(5-6), 235-320.

[128] Perlmutter, S., et al. (1999). Measurements of Omega and Lambda from 42 high redshift supernovae. The Astrophysical Journal, 517(2), 565-586.

[129] Planck Collaboration. (2018). Planck 2018 results. VI. Cosmological parameters. Astronomy Astrophysics, 641, A6.

[130] Alam, S., et al. (2017). The clustering of galaxies in the completed SDSS-III Baryon Oscillation Spectroscopic Survey: Cosmological analysis of the DR12 galaxy sample. Monthly Notices of the Royal Astronomical Society, 470(3), 2617-2652.

[131] Bennett, C. L., et al. (2013). Nine-year Wilkinson Microwave Anisotropy Probe (WMAP) observations: Final maps and results. The Astrophysical Journal Supplement Series, 208(2), 20.

[132] Smoot, G. F., et al. (1992). Structure in the COBE differential microwave radiometer first-year maps. The Astrophysical Journal Letters, 396, L1-L5.

[133] Hinshaw, G., et al. (2013). Nine-year Wilkinson Microwave Anisotropy Probe (WMAP) observations: Cosmological parameter results. The Astrophysical Journal Supplement Series, 208(2), 19.

[134] Guth, A. H. (1981). Inflationary universe: A possible solution to the horizon and flatness problems. Physical Review D, 23(2), 347.

[135] Peebles, P. J. E., Ratra, B. (2003). The cosmological constant and dark energy. Reviews of Modern Physics, 75(2), 559.

[136] Zaldarriaga, M., Seljak, U. (1997). An all-sky analysis of polarization in the microwave background. Physical Review D, 55(4), 1830.

[137] Kamionkowski, M., Kovetz, E. D. (2016). The quest for B modes from inflationary gravitational waves. Annual Review of Astronomy and Astrophysics, 54, 227-269.

[138] Hu, W., Dodelson, S. (2002). Cosmic microwave background anisotropies. Annual Review of Astronomy and Astrophysics, 40, 171-216.

[139] Bennett, C. L., et al. (2003). First-year Wilkinson Microwave Anisotropy Probe (WMAP) observations: Preliminary maps and basic results. The Astrophysical Journal Supplement Series, 148(1), 1.

[140] Planck Collaboration, et al. (2018). Planck 2018 results. VI. Cosmological parameters. Astronomy Astrophysics, 641, A6.

[141] Niemack, M. D., et al. (2010). The Atacama Cosmology Telescope: Instrumentation and data analysis. The Astrophysical Journal, 724(2), 1523.

[142] Ade, P. A. R., et al. (2016). Planck 2015 results. XIII. Cosmological parameters. Astronomy Astrophysics, 594, A13.

[143] Hinshaw, G., et al. (2013). Nine-year Wilkinson Microwave Anisotropy Probe (WMAP) observations: Cosmological parameter results. The Astrophysical Journal Supplement Series, 208(2), 19.

[144] Press, W. H.,Teukolsky, S. A., Vetterling, W. T., Flannery, B. P. (2007). Numerical recipes: the art of scientific computing (3rd ed.). Cambridge University Press.

[145] Akaike, H. (1974). A new look at the statistical model identification. IEEE Transactions on Automatic Control, 19(6), 716-723.

Contents lists available at ScienceDirect

New Astronomy

Cosmological test of $\frac{\sigma}{\theta}$ as function of scale factor in $f(R,T)$ framework

Himanshu Chaudhary, Aditya Kaushik *, Ankita Kohli

Department of Applied Mathematics, Delhi Technological University, Delhi 110042, India

ARTICLE INFO

ABSTRACT

The paper presents a study of the Bianchi type-I space–time model with perfect fluid in f(R, T) modified theory of gravity, where R is the Ricci scalar, and T denotes the trace of the energy–momentum tensor. The gravitational field equations of $f(R,T)$ are solved using expansion anisotropy as a suitable function of the average scale factor. Besides, we estimate the best-fit values of the model parameters by using the combined dataset of Cosmic Chronometers (CC) consisting of 31 measurements, the type Ia supernova dataset composed of 1048 measurements and the Baryon Acoustic Oscillations dataset consisting of ten measures with the Markov Chain Monte Carlo (MCMC) method. The resulting deceleration parameter shows that the Universe initially decelerated and later achieved an accelerated phase. Moreover, the paper analyses the cosmographic and cosmological parameters, suggest some improvements and illustrates findings through diagrams.

1. Introduction

In 1917 Einstein introduced the Cosmological Constant Λ in his field equations to ensure that his spatially spherical finite Universe was static and did not expand or contract over time. In 1922 Alexander Friedmann took two Einstein field equations and derived the two Friedmann equations, which showed how the Universe's spatial scale could change over time. In 1927/1929, Georges Lemaitre and Edwin Hubble observed the redshift of distant galaxies and concluded that the Universe was expanding. In 1964 discovery of Cosmic Microwave Background Radiation (CMB) by Arno Allan Penzias and Woodrow Wilson provided further evidence that expanding Universe and the big bang theory were correct based on observations of a supernova in 1998 from different periods in the Universe's history. We have determined that the Universe's expansion is accelerating, indicating that the Cosmological Constant Λ is small but positive. There are other astrophysical observations like Baryon Oscillation Spectroscopic (BAO) (Blake et al., 2011; Padmanabhan et al., 2012; Anderson et al., 2012), and PLANK Collaborations (Bennett et al., 2013) to confirm late time accelerating or expanding Universe since 1998. The Cosmological Constant Λ is sometimes called dark energy. It is often the case when Λ is on the left side of the Einstein Field Equation (EFE) along with the curvature term. However, in the trace reversed form of EFE, the Λ is on the right side of EFE along with the Energy Momentum Tensor (EM Tensor). Here Λ is responsible for the change in space–time geometry and can be considered an energy source. This type of energy is called Dark Energy. It does not appear to interact with light and is difficult to detect. Action principles are known to describe fundamental physical

theories. Instead of depending on our choice of coordinates, the metric action is intrinsic. The metric has a canonical volume form which we can multiply by any scalar function. Moreover, space–time is known to be a manifold M with a Lorentzian signature metric, and action is a part of M integrated across a manifold. Ricci Scalar R is the simplest of these functions. This action refers to the Einstein–Hilbert action. In $f(R,T)$ modified theory of gravity by Harko et al. Harko et al. (2011), R is the curvature scalar, and T is the trace of the Stress–Energy Momentum tensor. This theory is consequent to altering the Einstein–Hilbert Action (EH) (Buchdahl, 1970; Starobinsky, 1980; Nojiri et al., 2006; Nojiri and Odintsov, 2004, 2007; De Felice and Tsujikawa, 2010; Carroll et al., 2004; Capozziello et al., 2006; Chiba et al., 2007; Capozziello et al., 2008, 2019; Starobinsky, 2007; Nojiri and Odintsov, 2011; Bamba et al., 2012; Nojiri and Odintsov, 2003; Sotiriou and Faraoni, 2010; Capozziello and De Laurentis, 2011; Clifton et al., 2012; Bertolami et al., 2007). Their primary objective is to make sense of the late-time speeding up an extension of the Universe without requiring the presence of the cosmological constant Λ.

The day $f(R,T)$ modified theory of gravity was proposed, it has become one of the notable theories addressing different issues of theoretical cosmologists. Adhav (Adhav, 2012) derives exact solutions of the field equations in respect of LRS Bianchi type-I space–time filled with perfect fluid in the framework of $f(R,T)$ gravity and discusses the physical behaviour of the model. Neelima and Rao (Rao and Neelima, 2013) presents a study of spatially homogeneous and anisotropic Bianchi type-VI_0 space–time filled with perfect fluid in general relativity and in the framework of $f(R,T)$ gravity proposed by

---

* Corresponding author.

E-mail addresses: himanshuch1729@gmail.com (H. Chaudhary), akaushik@dtu.ac.in (A. Kaushik).

Menu   Search in thi: Submit your article ↗   Guide for authors ↗

Latest issue

Volume 103

In progress
October 2023

About the journal

An International Journal in
Astronomy and Astrophysics

New Astronomy publishes
articles in all fields of
astronomy and **astrophysic**

FEEDBACK 💬